RSC Advances

ROYAL SOCIETY OF CHEMISTRY

PAPER

View Article Online
View Journal | View Issue

Cite this: *RSC Adv.*, 2026, **16**, 20960

A new approach for the ultra-high loading of curcumin onto a nano-sized ZIF-68 as an effective drug delivery system with good biocompatibility and efficient anti-cancer therapy

Duy Ba Nguyen,[a] Phuong Bich Tran,[a] Quynh Ngoc Thi Luong,[a] Viet Ngoc Huynh,[a] Anh Ngoc Thi Phan,[a] Vu Tuyet Luu,[a] Duong Hoang Dang,[a] Hung Ngoc Nguyen,[a] Loc Cam Luu,[bd] Tan Le Hoang Doan [cd] and My Van Nguyen *[a]

Recently, metal–organic frameworks have become well-known as promising drug carrier systems for anticancer treatment. However, their performances are inadequate for real-life situations due to the uncontrolled drug release rate and lack of strong interactions between the backbone and guest molecules. To overcome these challenges, a nano-sized zeolite imidazole framework-68 was successfully prepared, denoted as ZIF-68, through the solvothermal technique, and demonstrated an extraordinary potential for curcumin (Cur) uptake. As a consequence, the maximum adsorption capacity and drug loading content of Cur over ZIF-68 reached 720.1 mg g^{-1} and 42.0%, respectively, which are much greater than those previously reported for drug carriers. These results best fit the Langmuir isothermal and pseudo-second-order models, indicating that the chemical interaction is dominant throughout the loading process. Furthermore, the Cur uptake mechanism is elucidated by the formation of robust attractions involving electrostatic interactions, π–π stacking, and hydrogen bonding between the drug molecules and the framework. This led to controlled drug release rates in human physiological medium (pH 7.4) and the tumor microenvironment (pH 5.0), thereby avoiding the "burst effect" at the initial stage. Remarkably, ZIF-68, after Cur loading (Cur@ZIF-68), was tested for cytotoxicity against HDF normal cells and MCF-7 cancer cells. As a result, Cur@ZIF-68 shows good biocompatibility with HDF cells and high cytotoxicity against MCF-7 cells at 25 μg mL^{-1}. These studies demonstrate that ZIF-68 is a promising candidate for an effective drug delivery system in anticancer therapy and support future research directions in designing porous materials capable of efficient drug carrying to support subsequent *in vivo* experiments.

Received 26th March 2026
Accepted 15th April 2026

DOI: 10.1039/d6ra02515c

rsc.li/rsc-advances

1. Introduction

In the past decades, anti-cancer drug consumption encountered several limitations in the treatment course, such as drug decline before reaching target cells, low selectivity, inadequate pharmacokinetics, and prolonged use demands.[1–3] Curcumin (Cur) is well-known as a type of promising therapeutic active ingredient, with properties including anti-cancer, anti-oxidant, anti-diabetic, *etc.*[4,5] In particular, Cur has the possibility to prevent the growth of many human cancer cell lines, involving breast, lung, gastrointestinal, and skin cancers.[6,7] Nevertheless, the therapeutic applications of Cur are restricted by low solubility in water, limited bioavailability, and fast metabolism.[8,9] Furthermore, the frequent and persistent use of the redundant Cur through ingestion causes serious threats to human health, as dysfunction of metabolic processes and stress increases.[10] Therefore, the advancement of a potential drug carrier system capable of replacing the conventional capsules and tablets to conduct the drug release, reduce the side effects, and promote its selectivity and biocompatibility, is urgent.[11–13] The drug nanocarriers have received much attention in order to deliver drugs effectively, such as hydrogels,[14] silica nanoparticles,[15] liposomes,[16] and polymeric/composite nanoparticles.[17–20] However, there are many obstacles to employing these stated drug carrier materials for efficient delivery in aspects of low drug uptake capacity, rapid relative drug release rate, and a lack of considerable affinity between the drug guest molecules and loading sites within the structure of the materials. Thus, it is imperative to seek a novel drug delivery system for efficiently

[a]*Faculty of Chemistry, Ho Chi Minh City University of Education, Ho Chi Minh City, 700000, Vietnam. E-mail: mynv@hcmue.edu.vn*
[b]*HCMC University of Technology, VNU-HCM, 268 Ly Thuong Kiet, District 10, Ho Chi Minh City, Vietnam*
[c]*Center for Innovative Materials and Architectures (INOMAR), Ho Chi Minh City, Vietnam*
[d]*Vietnam National University, Ho Chi Minh City, Vietnam*

capturing the drug molecules and overcoming the mentioned barriers. Recently, metal–organic frameworks (MOFs) have appeared as a dominant candidate for notable drug encapsulation and convenient drug release control with their extraordinary properties. MOFs are coordination polymeric materials with high porosity generated from organic ligands and metal ions/clusters *via* the coordination bonds and are applied in fields such as adsorption,[21–23] catalysis,[24–26] gas/vapour sensors,[27–30] energy storage,[31] and drug carriers[32,33] because of their adjusted and flexible architecture, large specific surface area, nano-sized crystallinity, good biocompatibility, and high thermal and chemical robustness.[34,35] Notably, the ligand moieties and metal clusters within MOFs can easily be modified by the functional groups for enhancing the drug uptake ability, biocompatibility, and reducing cytotoxicity.[33,36]

In fact, the priority criteria to choose MOFs as the drug carriers are whether they cause toxicity exceeding an acceptable degree to normal cells in the body. Hence, the metal ions, such as Zn^{2+}, Cu^{2+}, Mn^{2+}, and Fe^{3+}, naturally present in plasma and tissues, have been selected as precursors for MOF synthesis. Among these, Zn-containing MOFs are promising candidates and widely employed in the literature for drug delivery materials.[37–39] Considerably, zeolite imidazole framework (ZIF), a family of the MOF material constructed from imidazole/imidazole's derivatives and Zn^{2+} owing to unique performances, including high stability, facile modification, and low toxicity, is considered an effective drug transportation and targeted release carrier. Accordingly, Yu *et al.* fabricated ZIF-8-coated hyaluronic acid, demonstrating efficient Cur encapsulation and strong inhibition of breast cancer cells.[40] Additionally, Chotchindakun *et al.* used a ZIF-8 combined liposome layer as a Cur delivery carrier for enhanced biocompatibility and MCF-7 cell resistance with a low IC_{50} value.[41] Despite the advantages of the ZIF-8 platform for Cur delivery system, many challenges remain to be overcome. Consequently, the ZIF-8 platform can induce toxicity in normal cells at high concentrations, and exhibit a weak interaction with Cur molecules, and is merely the Cur adsorption on its surface, leading to limited loading capacity and an undesirable release rate, causing a "burst effect" at the initial stage of release.[37] Therefore, an approach using an extensive imidazole ring along with the polar nitro groups presented in the ligands to improve the strong attraction between the guest drug molecules and the ZIF backbone, incorporated with a suitable pore diameter to effectively capture the bulky architecture and large molecular size of Cur ($4.9 \times 7.9 \times 20.8$ Å), should be considered. It is interesting to note that ZIF-68, which possesses a fascinating structure, the appropriate pore size, a high specific surface area, and benzimidazole and nitro groups,[42] can enhance the interaction between Cur and the ZIF-68 framework and inhibit the drug burst effect. With this in mind, we hope that ZIF-68 will be used as a drug nanocarrier for efficient capture of Cur with high capacity and a controlled release rate. Additionally, using ZIF-68 as a Cur nanocarrier is considered an advantage in terms of synthetic process cost, as ZIF-68 can be synthesized in a simple one-pot process compared to the multi-stage preparation of other composite materials. This is a new pathway to cope with the aforementioned drawbacks of the ZIF-8 platform.

In this contribution, we employed ZIF-68 as a strategy for loading Cur with high capacity and conducted a release rate study. As expected, ZIF-68 showed excellent Cur uptake of 720.1 mg g^{-1}, with structural stability retained during the encapsulation process. The architectural characterizations of ZIF-68 and the uptake mechanism of Cur over ZIF-68 were interpreted through the analytical procedures combined with adsorption models. In addition, the pH-responsive Cur release of Cur@ZIF-68 was evaluated at pH 7.4 and 5.0, indicating the more effective release in an acidic medium. In particular, the biocompatibility and anti-cancer performance of ZIF-68 were confirmed through *in vitro* testing with normal and human breast cancer cell lines. As a consequence, the cell viability by ZIF-68 at a concentration of 25 μg mL^{-1} was about 74.2% for normal cells and 28.1% for the breast cancer cell line. These findings demonstrate the potential of ZIF-68 as an efficient Cur nanocarrier for future cancer treatment.

2. Experimental section

2.1. Chemicals and procedures

All the substances including zinc nitrate hexahydrate ($Zn(NO_3)_2 \cdot 6H_2O$, 98%), 2-nitroimidazole (2-nIm, 98%), benzimidazole (bIm, 98%), curcumin (Cur, 98%), *N*,*N*-dimethylformamide (DMF, 98%), methanol (MeOH, 99%), and ethanol (EtOH, 99%) were purchased from local suppliers.

Powder X-ray diffraction (PXRD) patterns were collected on a diffractometer (D8 Advance, Bruker) with Ni-filtered Cu Kα using a wavelength of 1.54718 Å. Raman spectra were measured on a spectrometer (XploRA ONE 532 nm, Horiba). Fourier transform infrared (FT-IR) spectra were obtained on a spectrophotometer (FT/IR-6600, Jasco). Scanning electron microscope (SEM) images were recorded on a microscope (FESEM S-4800, Hitachi) incorporated with energy-dispersive X-ray (EDX) mapping measured on an analyzer (EDX H-7593, Horiba). Thermal gravimetric (TG) analysis diagram was carried out on a thermal analyzer under dry air with the temperature range of 25–800 °C and heating rate of 10 °C min^{-1} (STA PT 1600, LINSEIS). Transmission electron microscopy (TEM) results were conducted on a microscope (JEOL 1010, Hitachi). X-ray photoelectron spectroscopy (XPS) was performed on an X-ray photoelectron spectrometer (PHI 5000, Chigasaki) equipped with a monochromatic Al Kα source operating at 50 W and 15 kV. The zeta potential and hydrodynamic diameter were measured on a zeta potential and particle size analyzer (SZ-100, Horiba). The nitrogen isotherm experiments were carried out on a 3Flex, Micromeritics at 77 K. UV-vis spectra were conducted on a spectrometer (Lambda 25, PerkinElmer).

2.2. Synthesis of ZIF-68

Based on the reported investigations,[42,43] a mixture containing 1.8 mL of $Zn(NO_3)_2 \cdot 6H_2O$ solution (0.2 M, 0.36 mmol), 5.4 mL of 2-nIm solution (0.2 M, 1.08 mmol), and 1.8 mL of bIm solution (0.2 M, 0.36 mmol) in DMF solvent with molar ratios of

1 : 3 : 1, respectively, was added to a 20 mL Pyrex vial. The mixture was then heated at 100 °C for 72 h. After cooling to room temperature, the product was centrifuged, washed with DMF for 48 h (30 mL per 24 h) to purge unwanted precursors, and exchanged with MeOH for 48 h (20 mL per 24 h). Subsequently, the sample was collected by centrifugation, dried, and activated under dynamic vacuum at 100 °C for 24 h to gain a light-yellow solid, denoted as ZIF-68 (85% yield, based on Zn^{2+}).

2.3. Drug loading studies

The Cur uptake investigations were carried out at room temperature with a stirring rate of 400 rpm. The Cur concentration in EtOH after capture over ZIF-68 was confirmed by a UV-vis spectrophotometer at 425 nm. The efficiency (%) and adsorption capacity (mg g^{-1}) at equilibrium (q_e) and intervals (q_t) of Cur were determined by the equations:

$$\text{Efficiency } (\%) = \frac{C_o - C_t}{C_o} \times 100 \quad (1)$$

$$q_e = \frac{C_o - C_e}{m} \times V \quad (2)$$

$$q_t = \frac{C_o - C_t}{m} \times V \quad (3)$$

where m (mg) and V (mL) are the material mass and the Cur solution volume. Whereas, C_o, C_t, and C_e are the Cur concentrations at original, t, and equilibrium time.

The different dosage (2–25 mg) of ZIF-68 was introduced to 40 mL of the Cur solutions (10 mg L^{-1}) to evaluate the optimal content. The uptake isotherms were conducted with the optimum dosage addressed, which was introduced into 40 mL of various initial concentrations of Cur (50–700 mg L^{-1}) and stirred for 24 h at room temperature. Furthermore, the loading kinetic models of ZIF-68 were observed at intervals from 15 to 150 min. In detail, a tested optimal content of ZIF-68 was immersed in 40 mL of the Cur solution of 30 mg L^{-1}, and stirred at the mentioned intervals. Particularly, to assess the drug loading content (DLC) and drug loading efficiency (DLE) parameters of ZIF-68, a series of experiments was conducted. Accordingly, 50 mg of the activated ZIF-68 was introduced to 40 mL of the Cur solution (700 mg L^{-1}) in EtOH and stirred at room temperature for 24 h. The solid was then centrifuged and washed with excess EtOH to remove the abundant Cur molecules anchored on the ZIF-68 surface. Continuously, the product was dried and activated under vacuum at 60 °C for 24 h to obtain a dark orange solid, termed Cur@ZIF-68. In order to calculate the DLC and DLE values, 3 mg of Cur@ZIF-68 was decayed in the mixture containing 0.75 mL of 2 M HCl and 30 mL of EtOH. The extraction was analyzed on a UV-vis spectrometer at a wavelength of 425 nm to determine the Cur content loaded in the ZIF structure based on the Cur standard curve and the equations for calculating the drug loading (Fig. S1 and Section S7). All adsorption experiments were conducted in triplicate.

2.4. *In vitro* drug release experiments

To gain initial insight into the pH-responsive performance of the material in the phosphate buffer solutions of pH 7.4 (physiological medium in the body) and 5.0 (survival condition of cancer cells), 5 mg of each Cur@ZIF-68 was soaked in 50 mL flask bottles, including 40 mL of phosphate buffer solutions containing 0.1% v/v Tween 80 at pH 7.4 and 5.0 separately. Subsequently, the mixture was put in a shaking incubator at 37 °C. After the specific intervals, 3 mL of the solution was withdrawn and refilled with 3 mL of a fresh solution of buffer and 0.1% v/v Tween 80 to restrict the saturated Cur and retain the same release conditions. After each time, the withdrawn solution was measured by a UV-vis spectrophotometer to indicate the content of the Cur released at various times. Moreover, the kinetic studies of release were surveyed. Consequently, the kinetic models such as zero order, first order, Higuchi, Korsmeyer–Peppas, and Hixson–Crowell were utilized to elucidate the drug release mechanism. The stated kinetic equations were detailed in the Section S8. All release studies were performed in triplicate.

2.5. Cell culture

The normal human dermal fibroblast (HDF) cells and the breast cancer cell line (MCF-7) were supplied from the American Type Culture Collection (ATCC, USA). The cells were suspended in Dulbecco's modified Eagle's medium (DMEM, Gibco) and introduced into 10% fetal bovine serum (FBS) and 1% v/v penicillin/streptomycin (P/S). The cells were then cultured in an incubator at 37 °C and 5% CO_2 in medium. As the cells grew and filled over 80% of the culture well plate surface, the culture environment was removed, and the cells were washed by PBS with pH 7.4 at least three times to totally detach the cell fragments. Subsequently, the cells were treated with 0.25% trypsin–EDTA solution (Gibco) for 5 min to separate them from the wells. After that, the cells were redistributed in the mixture of DMEM, 10% FBS, and 1% P/S. The cells were counted and seeded into 96-well culture plates with a density of 2.5×10^3 cells per well in an incubator for 24 h.

2.6. Cytotoxicity assay

The cell toxicity of ZIF-68, free Cur, and Cur@ZIF-68 on HDF and MCF-7 cell lines was determined by the 2-(4-iodophenyl)-3-(4-nitrophenyl)-5-(2,4-disulfophenyl)-2*H*-tetrazolium (WST-1) method through evaluation of the reduction level in cellular metabolism. In detail, the various concentration samples (1–30 μg mL^{-1}) in DMSO solvent were dispersed in DMEM medium with the presence of 1% P/S. After complete removal of the medium in the culture wells, the cells were incubated in the sample solutions with the prepared different concentrations for 24 h. Continuously, 10 μL of WST-1 reagent solution was introduced into each well and placed in the incubator for 2 h. The absorbance of the reaction solution in each well was then analyzed at 450 nm using a microplate reader (Tecan Group, Switzerland). Herein, the cell viability (%) was calculated by the percentage recorded from the fluorescence intensity of treated

cells in comparison with untreated cells, according to the following equation:

$$\text{Cell viability } (\%) = \frac{OD_{sample} - OD_{blank}}{OD_{control} - OD_{blank}} \times 100 \quad (4)$$

where OD_{sample}, $OD_{control}$, and OD_{blank} are the optical density of cells treated with the sample, DMEM, and pure DMEM medium without the cells, respectively.

Besides, the morphology and viability of the HDF cells were studied by a Live/Dead assay kit through calcein acetoxymethyl (AM) staining procedure. After the cells were treated with the Cur@ZIF-68 samples at various concentrations, such as 0, 10, 25 μg mL^{-1}, similar to the mentioned cytotoxicity assay, the cells were incubated with 100 μL of PBS solution containing 2 μM calcein-AM and 4 μM ethidium homodimer-1 for 15 min. The fluorescence microscope (Nikon, Japan) was then employed for survey. All cytotoxicity assays were also conducted in triplicate.

2.7. Statistical analysis

The data were figured statistically significant with $p < 0.05$ (*), $p < 0.01$ (**), $p < 0.001$ (***), and ns: no significant. Furthermore, the IC_{50} values were estimated from the dose–response graph with the dependence between the logarithm of sample concentration and cell viability. The number of replicates was 3 for all experiments.

3. Results and discussions

3.1. Fabrication and full characterization of ZIF-68

To enhance the adsorption capacity of Cur and control the drug release rate, a strategy of the ZIF synthesis with the appropriate pore diameter, and effective interaction between the framework and drug guest molecules has been proposed. With all this considered, a stock solution of 2-nIm and bIm linker, and $Zn(NO_3)_2 \cdot 6H_2O$ salt was heated at 100 °C for 3 days to achieve a light yellow solid.

Subsequently, the product was washed with DMF to purge the unreacted precursors and exchanged with excess MeOH to facilitate the removal of solvent during activation under mild conditions. The solid was then dried and activated upon vacuum at 100 °C for 1 day to detach the solvent from the backbone and obtain a pure product, namely ZIF-68 (Fig. 1). Herein, ZIF-68 is composed of the clusters of ZnL_4 tetrahedral type generated at the original stage of the reaction, and two of the 2-nIm and bIm ligands to form the three-dimensional architecture with GME topology. The GME topology of ZIF-68 was well-known as a beautiful topology mode with a large pore size, attractive surface area, and bearing the moieties of benzene rings and nitro groups,[42] which is suitable for high loading possibility of Cur *via* the strong interaction between the Cur guest molecules and the ZIF framework, leading to an efficient control for the drug release process.

To access the phase purity degree of ZIF-68, the powder X-ray diffraction (PXRD) analysis is performed. As a result, the PXRD pattern of the activated ZIF-68 sample is in a good agreement with the simulated structure (CCDC 671075) through high correspondence of the lattice planes including (1 0 0), (1 0 1), (2 −1 0), (2 0 0), (0 0 2), (3 −1 0), (3 −1 1), and (4 −2 0) (Fig. 2a). Raman spectra of ZIF-68 and the linkers are revealed in Fig. 2b. Accordingly, the characteristic vibrational modes at 1121/1163, 1294, 1367/1406, and 1480 cm^{-1} are assigned to δ_{C-H} (out of plane), δ_{C-H} (in plane), ν_{C-N}, and $\nu_{C=N/C=C}$, respectively, in the presence of ZIF-68 but appeared at different positions for two of 2-nIm and bIm linkers. In addition, the $\nu_{C=N/C=C}$ band of the benzene ring at 1587 cm^{-1} appears in both bIm and ZIF-68 samples, whereas the existence of the characteristic signal at 1545 cm^{-1} is attributed to the absorption mode of asymmetric $-NO_2$ groups inside the ZIF-68 and 2-nIm spectra.[44,45] Also, the FT-IR spectra of the samples are clearly displayed in Fig. 2c. As expected, the main characteristic bands, such as the asymmetric nitro, C=N/C=C, symmetric nitro, C–N, C–N–C stretching, and ring deformation mode (out of plane) at 1537, 1482, 1363, 1168, 1004, and 653 cm^{-1}, respectively,[46,47] are revealed in the ZIF-68 spectrum, but located at the various wavelengths in the linker spectra. This phenomenon can be accounted for by the generation of coordination bond networks between inorganic and organic moieties within the ZIF architecture in comparison to the initial individual components and exhibits a high correlation with the results observed in Raman analyses.

To obtain a deeper understanding of the unique properties of ZIF-68, a series of additional measurements, including TGA, SEM-EDX-mapping, TEM, 77 K N_2 sorption, zeta potential, particle size, and XPS, were conducted on the activated ZIF-68. As a consequence, the TGA diagram is analyzed in a dry air medium and specifically shown in Fig. 2d. A small weight decrease of 6.7% is assigned to the loss of residual solvent in the pores and absorbed water molecules on the surface of ZIF-68 from room temperature to 300 °C. Next, a significant loss (81.2 wt%) from 300 to 800 °C is attributed to the decomposition of the framework corresponding to the release of moiety caps and linker within ZIF-68. This proves that the backbone of ZIF-68 can withstand temperatures up to 300 °C, which is relevant for further applications in harsh conditions.

Besides, the N_2 isotherm of ZIF-68 at 77 K indicates a desirable value with a BET surface area of 1098 $m^2\ g^{-1}$ (Fig. 3a). The pore size distribution reveals a dominant window pore diameter of approximately 22 Å. With the Cur molecule size (4.9 × 7.9 × 20.8 Å), the pore size of ZIF-68 is quantitatively sufficient to encapsulate curcumin molecules. This spatial compatibility, combined with the high surface area, facilitates effective capture and high Cur loading capacity within the ZIF-68 backbone. In particular, the SEM and TEM images exhibit that the particles of ZIF-68 have the shape of polyhedron blocks with a relatively uniform distribution of the average size in the range of 150–200 nm (Fig. 3b–e). To further confirm the morphology of the material, the EDX-mapping analysis was also conducted. Accordingly, the dominant existence of the elements on the ZIF-68 surface is clearly displayed (Fig. S2). This evidence shows a high single-phase level of the fabricated material.

Remarkably, the XPS measurements reveal the complete appearance of C, N, O, and Zn constituents in ZIF-68 (Fig. 4a). The high-resolution XPS data were collected to interpret the

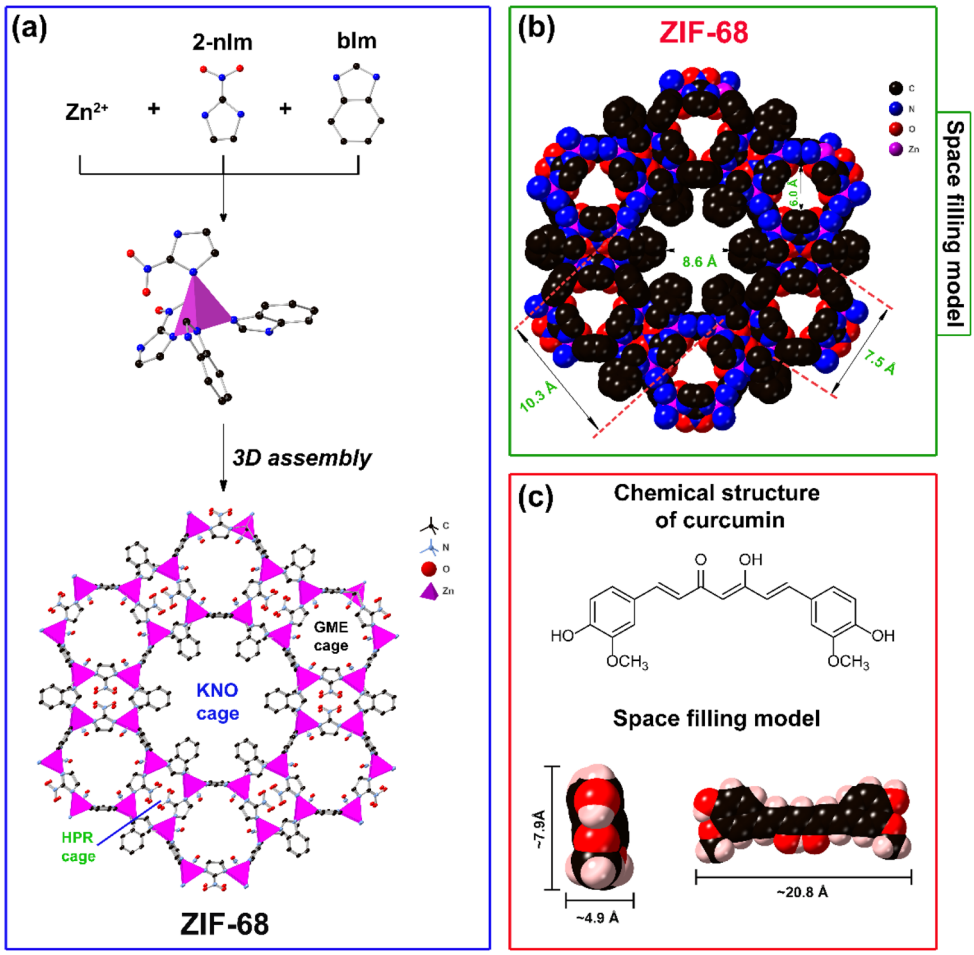

Fig. 1 The architectures of ZIF-68 are generated by ZnL_4 tetrahedral and the linkers of 2-nIm and bIm (a); space filling model of ZIF-68 (b); chemical structure of curcumin (c). Atom colors: Zn, pink polyhedra; C, black; O, red; N, blue; H, off-white.

binding energy of bonds and the oxidation states of each element within the material. The high-resolution C 1s core of ZIF-68 indicates the peaks at 284.7 and 286.8 eV, assigned to the C═C/C–C and C–N/C═N bonds, respectively (Fig. 4b). In the N 1s spectrum, the various signals at 393.3, 401.1, and 406.0 eV are accounted for the presence of the N–C, N═C, and N–O bonds, respectively, with the corresponding percentage contribution in Fig. 4c. In addition, in Fig. 4d, the O 1s curve is deconvoluted into the two distinctive contributions at 532.3, and 535.4 eV, respectively, derived from the O–N and absorbed water due to the exposured ZIF-68 process.[48,49] Especially, the Zn 2p band is divided into the two peaks of Zn moieties, as denoted, 1021.9, and 1045.0 eV, corresponding to Zn $2p_{3/2}$, and Zn $2p_{3/2}$, respectively (Fig. 4e).[49]

In order to evaluate the zeta potential and particle size of ZIF-68, the dynamic light scattering (DLS) method was performed. It is interesting to note that the zeta potential of the materials functionalized by nitro groups becomes more negative in an aqueous medium.[50] As expected, nitro-containing ZIF-68 possesses a negative zeta potential of −64.9 mV (Fig. 5a), which is impressive in forming an efficient attraction between the negative surface of ZIF-68 and the polar groups, including the keto/enol moieties of the Cur molecules.

Thus, the zeta potential of Cur@ZIF-68 is −23.1 mV (Fig. 5b), which is reasonable and proves the successful encapsulation of Cur onto the pores of ZIF-68 *via* the stated interactions. These high absolute zeta potential values exhibit a good colloidal robustness, and aggregation decrease in serum, resulting in the remarkable support for the drug delivery.[51] The fact reveals that the nanoparticles with size in the range of 50–300 nm will enhance the ability of tumor tissue accumulation for the cancer treatment *via* the enhanced permeability and retention (EPR) effect, which is much more effective than free Cur.[52] Consequently, the particle size of ZIF-68 is confirmed by the DLS analysis to be 131.4 ± 29.4 nm (Fig. 5c), which is no significant difference in comparison with the mentioned TEM data. Meanwhile, after loading of Cur, the particle size of Cur@ZIF-68 rises to 252.9 ± 33.8 nm, which is a common situation in the drug-loaded nanocarriers.[53] This phenomenon can be explained by the fact that the Cur molecules are uptaken on the surface and anchored in the pores of ZIF-68, causing an increase in the hydrodynamic diameter. All of the observations mentioned above, obtained from modern and highly reliable analytical

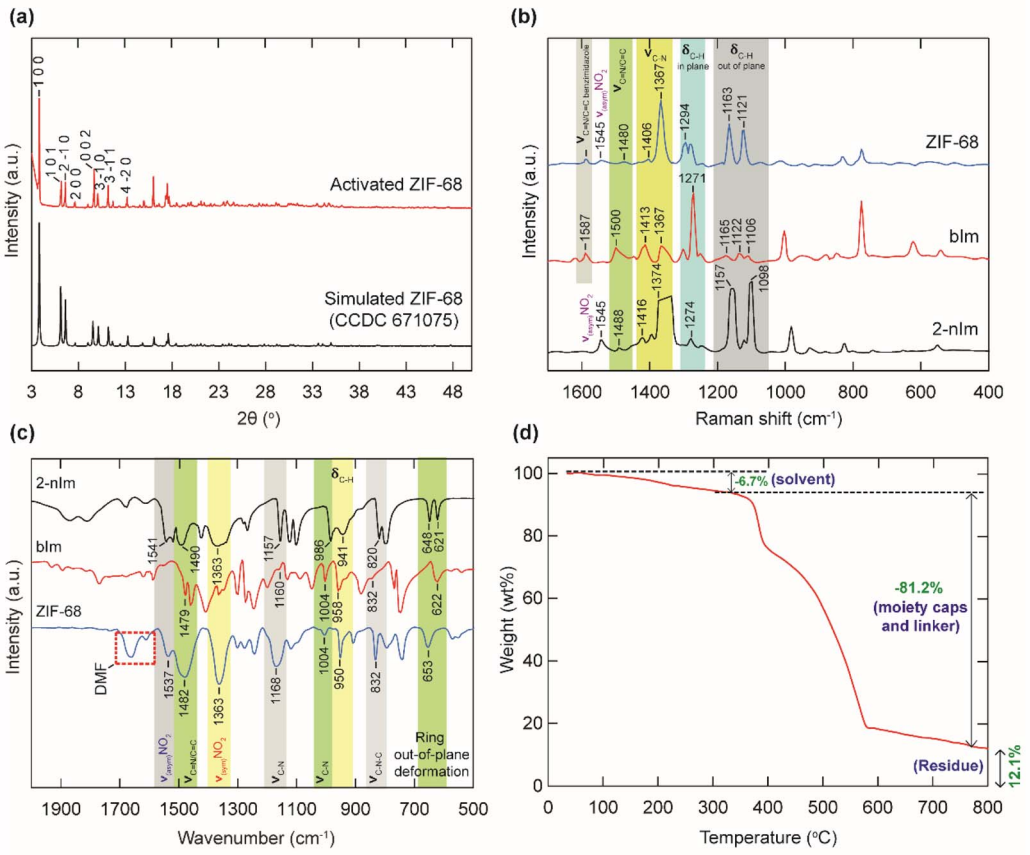

Fig. 2 Powder X-ray diffraction analysis of activated ZIF-68 (red) in comparison with the simulated ZIF-68 (black) (a); Raman spectra of 2-nIm linker (black), bIm linker (red), and ZIF-68 (blue) (b); Fourier transform infrared spectra of 2-nIm linker (black), bIm linker (red), and ZIF-68 (blue) (c); TGA diagram of activated ZIF-68 (d).

methods, demonstrate that the ZIF-68 material has been successfully prepared in terms of high uniformity and phase purity, which are conducive to carrying and delivering Cur effectively for anti-cancer treatment.

3.2. Drug uptake investigations

To study the ideal dosage of ZIF-68 for the encapsulation process of Cur onto the material, the various contents (2–25 mg) of ZIF-68 were introduced into 40 mL of the Cur solution in EtOH with a concentration of 10 mg L^{-1}, and stirred with a constant rate at room temperature for 24 h.

As exhibited in Fig. 6a, the uptake efficiency of Cur increases from 21 to 98% with the dosage change from 2 to 15 mg, respectively. This difference can be accounted for by the increase in the material's content, leading to more adsorptive sites and cavities for the Cur capturing. When the ZIF-68 dosage reaches about 20–25 mg, the Cur uptake changes insignificantly by about 0.3%, indicating a generated encapsulation balance. Therefore, the optimal content of 15 mg is utilized for the subsequent studies.

In order to point out the nature of the Cur adsorption over ZIF-68, the uptake isothermal models were used to detail the interaction between the Cur molecules and the framework. As illustrated in Fig. 6b, the Cur adsorption capacity is promptly boosted with an increase in the Cur initial concentration from 50 to 500 mg L^{-1}. This can be ascribed to the enhancement of the adequate adsorption sites within ZIF-68 to effectively encapsulate Cur. Meanwhile, the uptake capacity reaches an equilibrium value as the Cur concentration increases from 500 to 700 mg L^{-1}, which is attributed to the complete filling of the Cur molecules inside the pores of ZIF-68. Next, the isothermal models, including Langmuir, Freundlich, Temkin, and Dubinin–Radushkevich (DR), were employed. The linear forms of the stated isothermal equations are indicated in Section S7. Fig. 6c–f shows the linear fitting plots of the Cur uptake models onto ZIF-68. As given in Table S1, the fitting coefficient of the Langmuir model ($R^2 = 0.996$) is greater than those of the Freundlich, Temkin, and DR models with *R*-squared values of 0.960, 0.982, and 0.769, respectively. In addition, the maximum Cur adsorption capacity is 720.1 mg g^{-1} recorded from the isothermal curve (Fig. 6b), which is reasonable as compared to the theoretical value derived from the Langmuir model (833.3 mg g^{-1}). This difference can be attributed to steric hindrance between the Cur molecular size and the ZIF-68 pores, which prevents 100% theoretical monolayer coverage. The obtained evidence reveals that the Cur monolayer uptake onto the material is created at the boundary between ZIF-68 and the guest molecules. Moreover, the separation value of R_L is

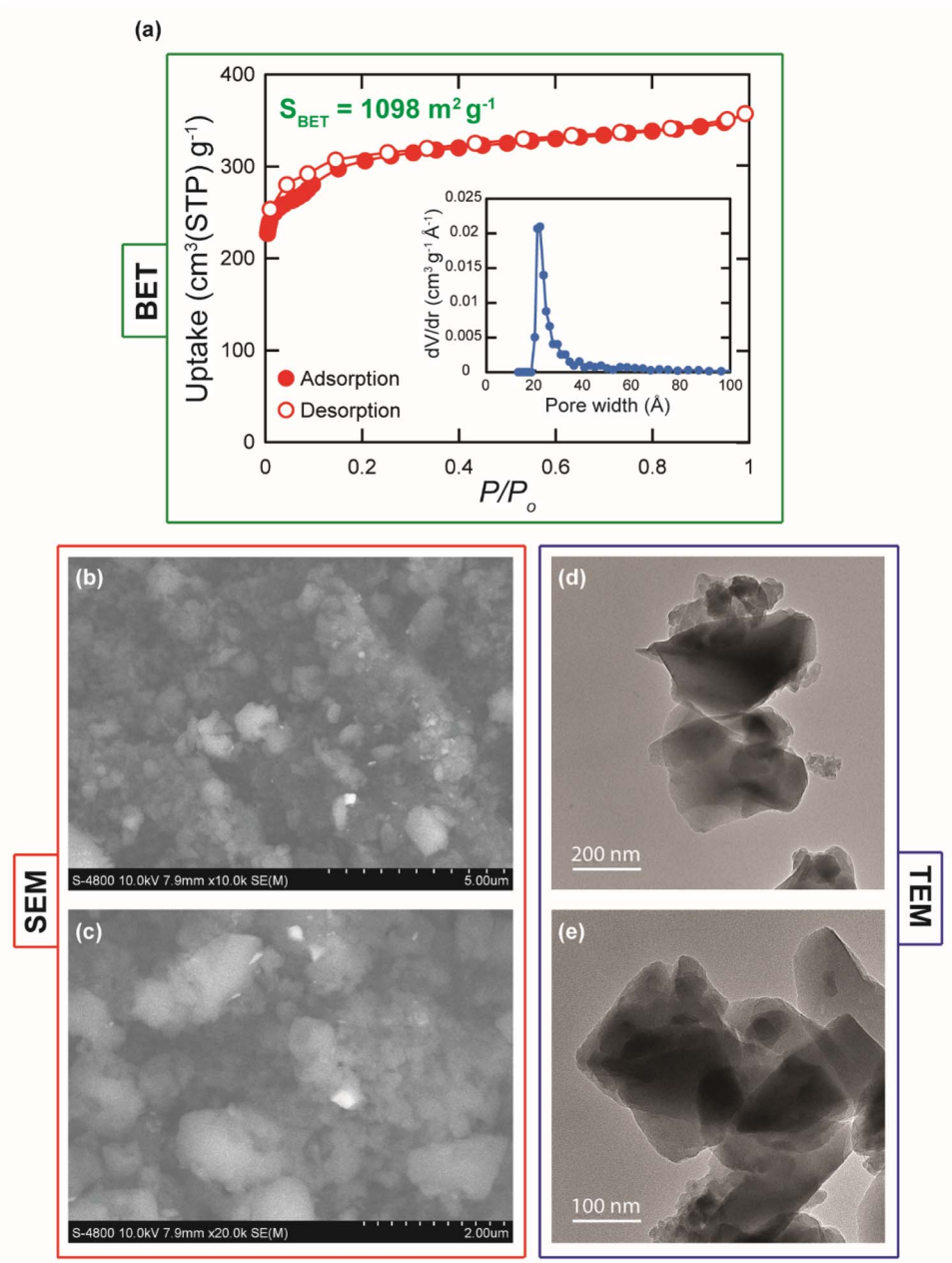

Fig. 3 N_2 isotherm at 77 K for activated ZIF-68 (a): closed and open circles represent the adsorption and desorption branches, respectively. Inset: the plot of the pore size distribution of ZIF-68. SEM image of ZIF-68 at a scale bar of 5 μm (b) and 2 μm (c); TEM image of activated ZIF-68 at a scale bar of 200 nm (d), and 100 nm (e).

inferred from the Langmuir model in Section S2, considered as a vital factor to assess the capturing convenience. In detail, the gained R_L parameter is acceptable ($0 < R_L < 1$) to demonstrate an irreversible and advantageous anchoring of Cur over ZIF-68. This can be argued by the formation of the effective interaction of the active adsorption centers within ZIF-68 and the Cur molecules *via* the attraction of the conjugated π electron clouds, hydrogen bond system, and electrostatic attraction generated during the encapsulation.[54,55]

Besides, the adsorption kinetic experiments were surveyed to further elucidate the Cur uptake mechanism onto ZIF-68. As shown in Fig. 7a, the uptake capacity of Cur over ZIF-68 increases rapidly after the first 90 min and achieves the balance value in 120 min. Subsequently, the uptake kinetic models, including pseudo-first-order and pseudo-second-order, were used (see eqn (S8) and (S9)). The pseudo-first-order model indicates that the absorbent surface is affected by the uptake rate. Whereas the pseudo-second-order model exhibits a strong attraction between the active sites within the material and the guest components.[21] Accordingly, the *R*-squared values of the pseudo-first-order and pseudo-second-order models are 0.986

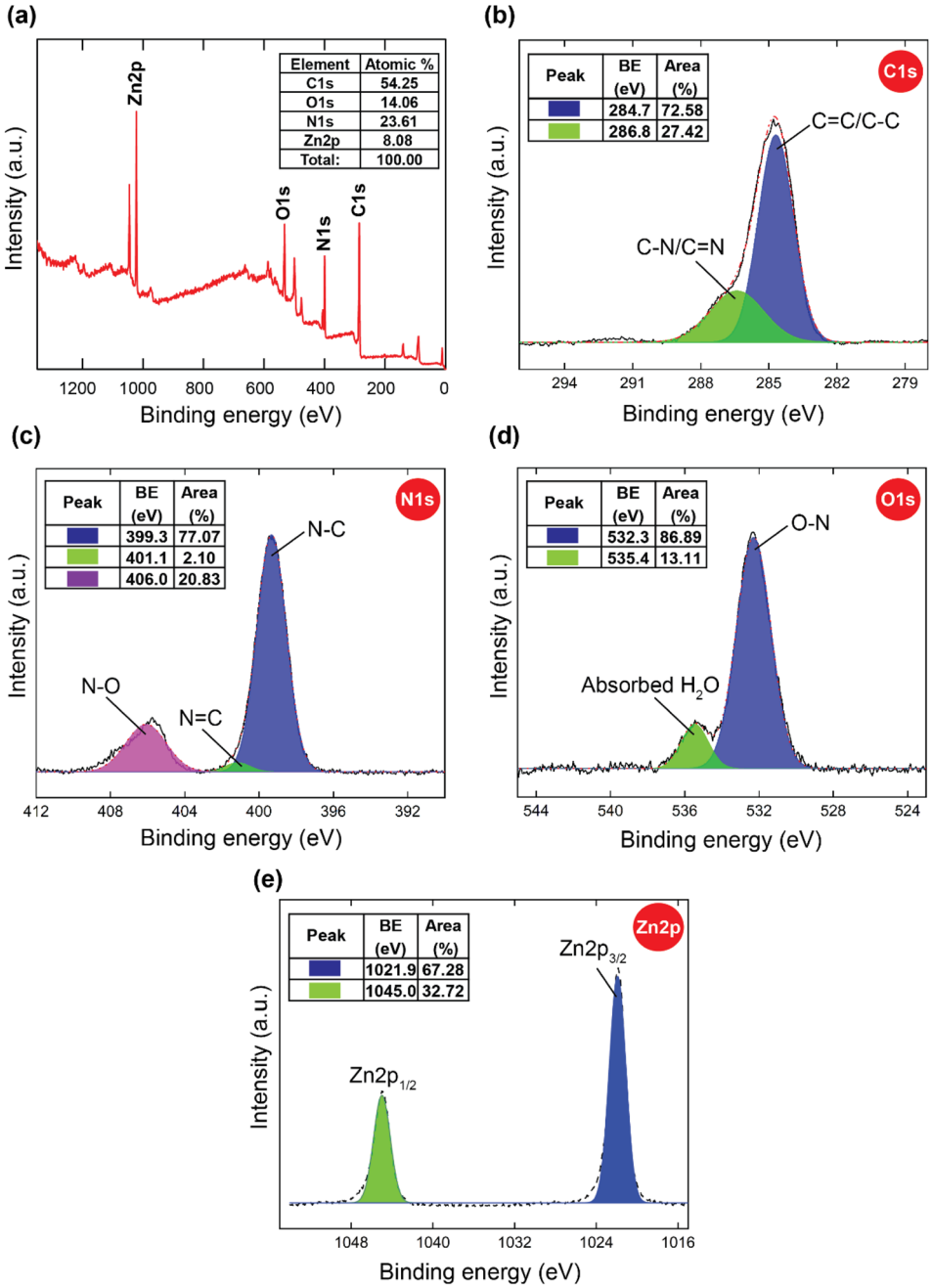

Fig. 4 The XPS measurement of ZIF-68: the XPS survey (a); high-resolution spectrum of C 1s (b); high-resolution spectrum of N 1s (c); high-resolution spectrum of O 1s (d); high-resolution spectrum of Zn 2p (e).

and 0.998, respectively, and are clearly revealed in Fig. 7b, c, and Table S2.

Based on these data, the Cur encapsulation onto ZIF-68 is consistent with a process dominated by chemical interactions, supported by efficient π–π stacking, electrostatic interactions, and hydrogen-bonding networks formed between the ZIF backbone and Cur. To further affirm the unique performance of ZIF-68, the maximum Cur uptake capacity of the material was compared with that of the other carriers in Table S3. Accordingly, ZIF-68 possesses a much greater adsorption ability than the other Cur delivery materials. On the other hand, the structural robustness of the drug delivery material after the encapsulation plays a vital role in considering the economic effectiveness of the nanocarrier in terms of storing and preserving medicines for prolonged periods. Consequently, ZIF-68 after the Cur uptake was washed with EtOH to remove the Cur molecules remaining on the ZIF surface, dried, and activated under vacuum at 80 °C for 24 h. The sample was then kept for 1 month under ambient conditions. Continuously, the architectural stability of the stored Cur@ZIF-68 was inspected by the PXRD, FT-IR, SEM, and TEM procedures. As exhibited in Fig. S3, the PXRD patterns of the activated ZIF-68 and the

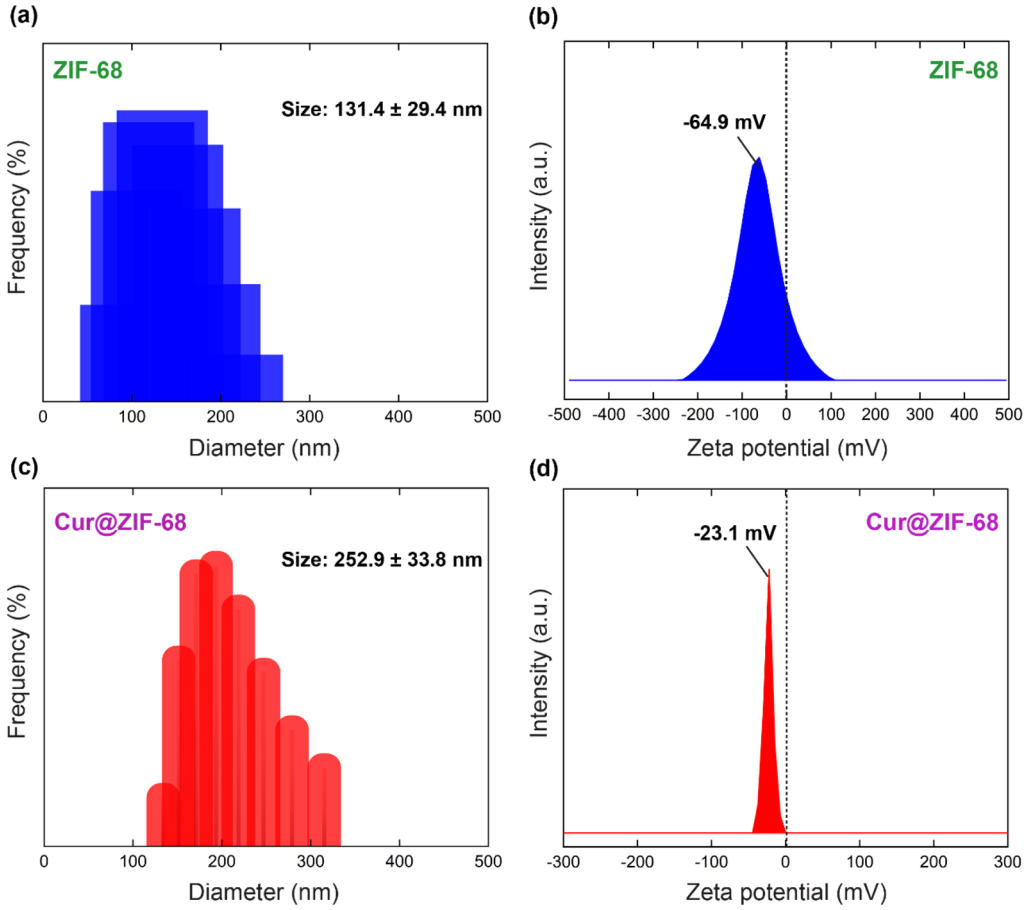

Fig. 5 The hydrodynamic diameter (a) and zeta potential (b) of ZIF-68; the hydrodynamic diameter (c) and zeta potential (d) of Cur@ZIF-68.

preserved Cur@ZIF-68 sample indicate a good accordance, confirming a high stability of Cur@ZIF-68 in the practical medium. Next, the FT-IR spectrum of Cur@ZIF-68 displays the characteristic bands retained throughout the encapsulation as compared to the pristine ZIF-68 (Fig. S3). Also, the surface morphology and particle size of the nanocarrier show no considerable change after the uptake, as clearly illustrated in the SEM and TEM analyses (Fig. S3). These gained observations highlighted that ZIF-68 could be applied as a potential drug carrier under actual storage and circulation conditions.

3.3. Plausible uptake mechanism

Owing to the existence of the applicable pore size and high-density conjugated π electron system of the linkers within ZIF-68, the capturing mechanism of Cur over ZIF-68 can be proposed by the creation of the π–π interactions, hydrogen bonding system, and electrostatic attractions. To inspect this assumption, we carried out extensive measurements such as FT-IR, Raman, and XPS. Accordingly, the FT-IR spectrum of Cur@ZIF-68 shows the shift to the other frequencies of the characteristic bands of asymmetric nitro groups, $\nu_{C=N/C=C}$, and ν_{C-N} at 1499 and 1159 cm^{-1}, respectively, as compared to the pristine ZIF-68 spectrum (Fig. 8a).

Particularly, the presence of two new vibrational modes at 1594 and 1612 cm^{-1} in the Cur@ZIF-68 spectrum is assigned to the C=O stretching vibration of the Cur molecules anchored into the pores of the material. This situation can be described by the generation of the considerable interaction between the hydroxyl groups, benzene rings of the Cur molecules, and the active uptake centers, including the electron-rich nitrogen sites of N-heterocyclic in both linkers, nitro groups of 2-nIm and benzene ring of bIm within ZIF-68.[55,56] Raman spectroscopy of the Cur@ZIF-68 sample was also analyzed to further confirm the Cur efficient encapsulation onto the ZIF framework. As given in Fig. 8b, the reasonable appearance of the C=O characteristic signal related to the Cur molecules at 1628 cm^{-1} within Cur@ZIF-68, which is similar to the stated FT-IR result and proves the successful capturing of Cur into the material's architecture.

Furthermore, the vibrational modes at 1118, 1356, 1487, and 1594 cm^{-1}, corresponding to the bonds of C–H (out of plane), C–N, C=N/C=C, and C=N/C=C in bIm, respectively, exist in the Cur@ZIF-68 sample,[44,56] but are located in the various regions in the pure ZIF-68 range. This finding again confirms the main formation of the hydrogen bonding system and π–π interactions between the backbone and guest moieties. The uptake mechanism was further elucidated with XPS

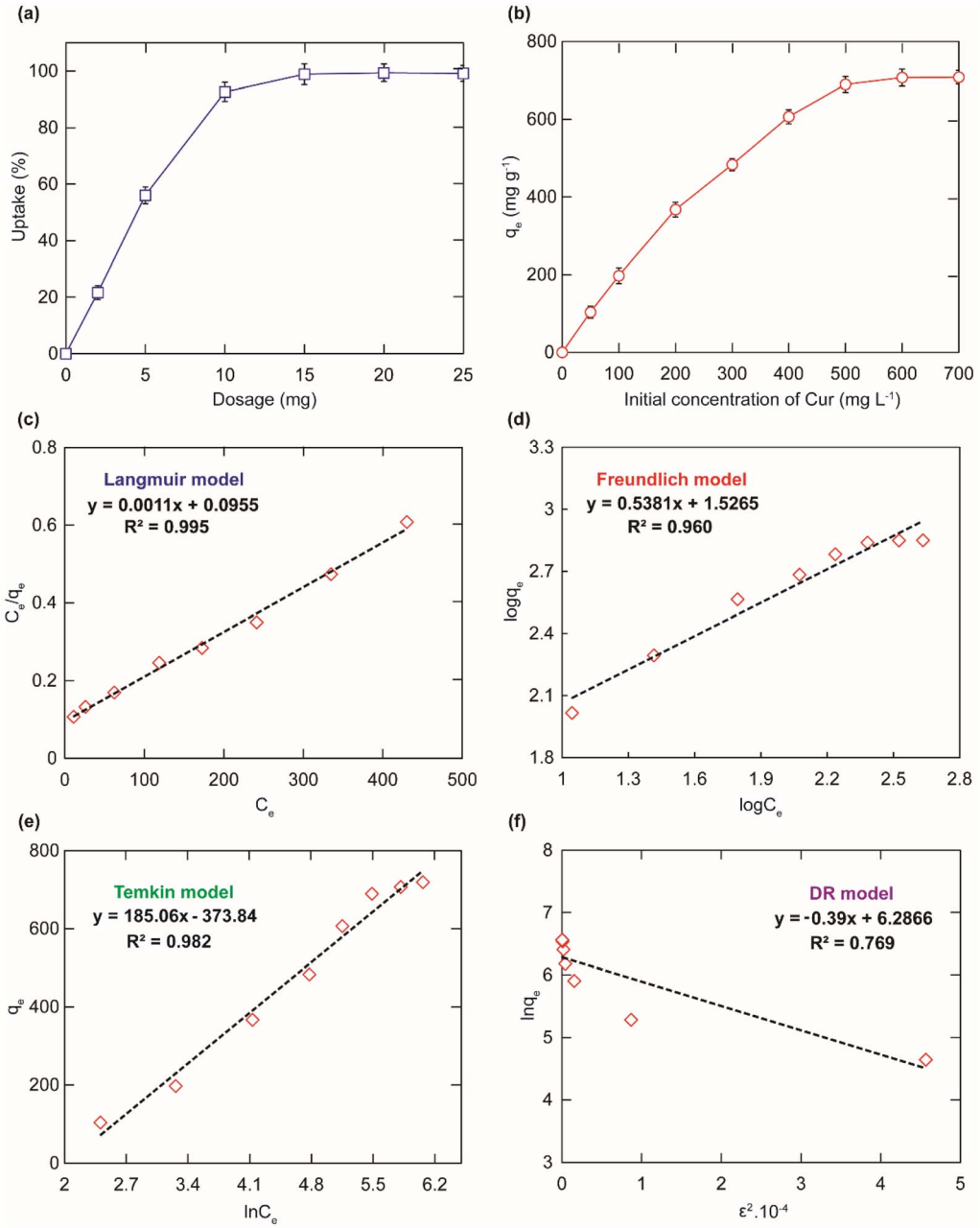

Fig. 6 Influence of ZIF-68 content on the Cur uptake (a) [m = 2–25 mg, V = 40 mL, C_o: 10 mg L^{-1}, t = 24 h]; effect of the initial concentration on the Cur loading capacity (b) [m = 15 mg, V = 40 mL, C_o: 50–700 mg L^{-1}, t = 24 h]. Data fitting with the isothermal models: Langmuir (c), Freundlich (d), Temkin (e), and DR (f).

measurement. Fig. 8c shows the appearance of the components such as C, N, O, and Zn inside the Cur@ZIF-68 material, like the XPS analysis of the pristine ZIF-68. However, the high-resolution spectra of Cur@ZIF-68 exhibit the displacement of binding energies for each element in comparison with the pure ZIF-68 sample. Consequently, the C 1s core of Cur@ZIF-68 is divided into three signals located at 284.0 and 286.5 eV, which are assigned to the C=C/C–C and C–N/C=N bonds, respectively (Fig. 8d). Interestingly, these peaks are moved to different ranges in relation to the parent ZIF-68 (284.7 eV for C=C/C–C, and 286.8 eV for C–N/C=N) (Fig. 4b).[49] Notably, a new signal of C=O is found in Cur@ZIF-68 at 284.9 eV, but is absent in the ZIF-68 spectrum, which proves the Cur settlement into the pores of ZIF-68.[57] The high-resolution N 1s curve is deconvoluted into three characteristic peaks at 399.0 eV, 400.2 eV, and 405.8 eV with the corresponding percentage of area in Fig. 8e, relating to the N–C, N=C, and N–O,[40] respectively, similar to the signals collected in the ZIF-68 sample, but occupied at the various positions. This affirms that the outstanding attraction is generated between the N-heterocyclic and N sites of the framework and Cur. Additionally, the O 1s spectrum of Cur@ZIF-68 indicates the essential peaks at 532.6 and 535.2,

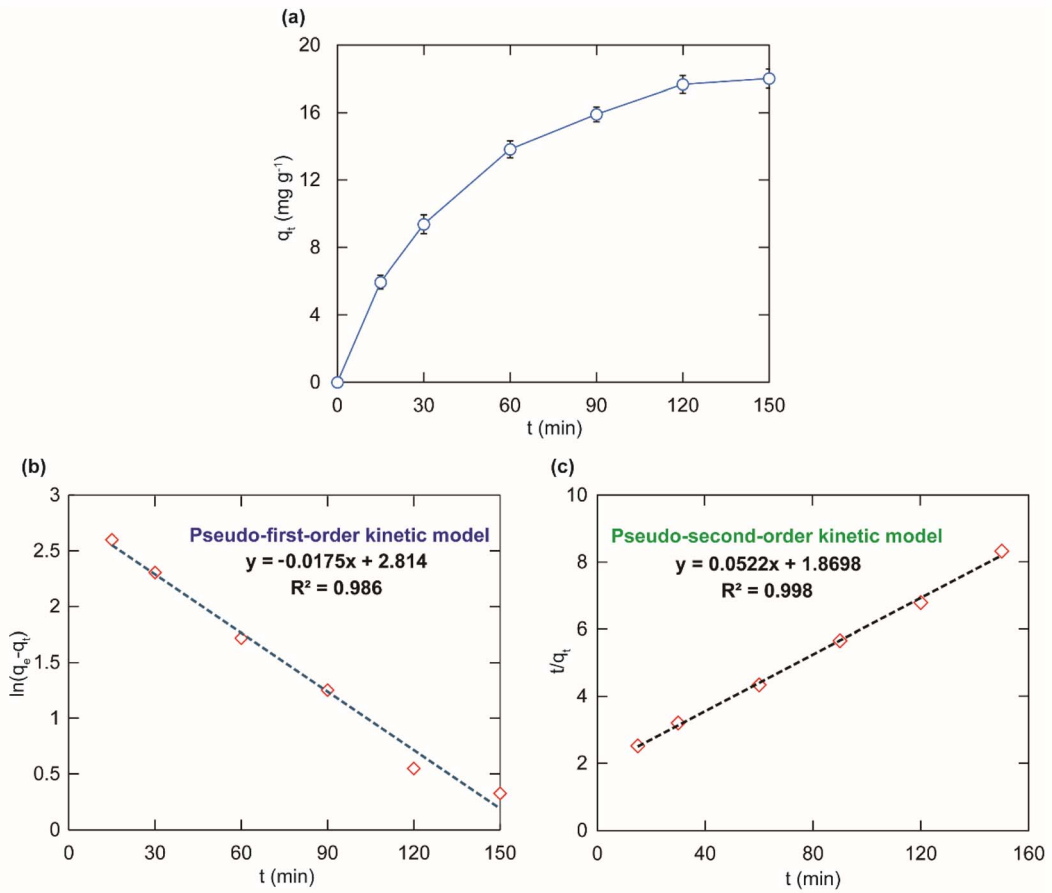

Fig. 7 The kinetic data for the Cur uptake over ZIF-68 (a) [$m = 15$ mg, $V = 40$ mL, $C_o = 30$ mg L^{-1}, $t = 15$–150 min]; fitting results with the Cur uptake kinetic models: pseudo-first-order (b), pseudo-second-order (c).

corresponding to the N–O and adsorbed H_2O binding energies, which is comparable to the ZIF-68 spectrum (Fig. 8f).

Noteworthily, in the Cur@ZIF-68 spectrum, there is a new signal at 531.8 eV, corresponding to the C═O bond within the material, demonstrating the prosperous anchoring of Cur onto ZIF-68. Apart from the mentioned crucial interactions, including the hydrogen bondings formed by the electron-rich nitro groups with the phenolic and enol-type hydroxyl groups, and π–π stackings, a hypothesis regarding the generation of the electrostatic interactions between the hydroxyl and β-ketone moieties inside Cur and the Zn^{2+} tetrahedral species within ZIF-68 has been suggested. As a consequence, the Zn 2p spectrum of ZIF-68 after the Cur encapsulation reveals the movements to the lower binding energy peaks, such as 1021.5 eV for Zn $2p_{3/2}$ and 1044.6 eV for Zn $2p_{1/2}$ (Fig. S4) in contrast to the pure ZIF-68 sample (Fig. 4e). This implies that the formation of the considerable electrostatic interaction of the electron-rich groups in Cur along with the Zn^{2+} moieties within the ZIF backbone during the capture of Cur. This case is also observed in the previously reported literature.[56] These findings demonstrate that the ultra-high uptake capacity of Cur over ZIF-68 is supported by the strong attractions, involving hydrogen bonding networks, π–π, and electrostatic interactions (Scheme 1). This is one of the important factors to using Cur@ZIF-68 as an effective drug carrier for the subsequent *in vitro* testing to treat cancer cells.

3.4. *In vitro* drug release experiments

In fact, the burst effect occurred during the drug release process of nanocarriers causes the limitations, including the increase of local cytotoxicity risk due to a large number of drug molecules released at the original stage, the decline of durable therapeutic efficiency, the difficulties in controlling the drug concentration in the range of the optimal treatment, and causing to the deviation of the desired drug release kinetic.[58] Owing to the stated obstacles, the design strategy of the Cur delivery material capable of controlling drug release kinetics *via* the optimal pore size engineering and the enhancement of intermolecular attractions between Cur and the ZIF structure to cope with the burst phenomenon has been approached. As mentioned in the Cur uptake mechanism, ZIF-68 has emerged as a promising candidate for controlled Cur release from the architecture. Hence, a series of investigations was conducted to explore the Cur release of Cur@ZIF-68. In detail, 15 mg of ZIF-68 was added to 40 mL of the Cur solution with a concentration of 700 mg L^{-1}. The mixture was stirred at room temperature with a constant

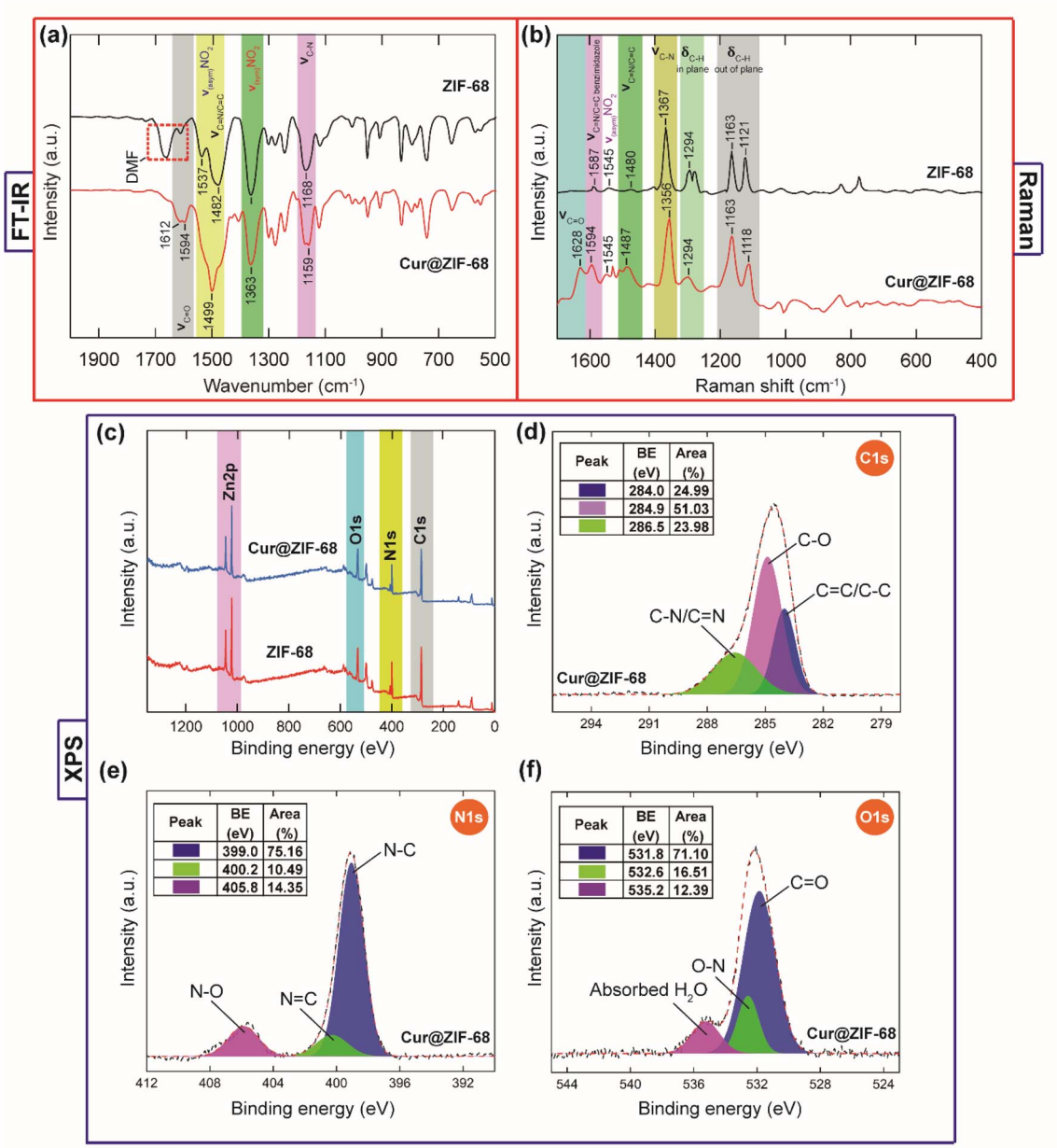

Fig. 8 The FT-IR spectroscopy of activated ZIF-68 (black) in comparison with Cur@ZIF-68 (a); Raman spectra of activated ZIF-68 (black) and Cur@ZIF-68 (red) (b); the XPS analysis of Cur@ZIF-68: the XPS survey of Cur@ZIF-68 (blue) as compared to ZIF-68 (red) (c); high-resolution spectrum of C 1s in Cur@ZIF-68 (d); high-resolution spectrum of N 1s in Cur@ZIF-68 (e); high-resolution spectrum of O 1s in Cur@ZIF-68 (f).

rate for 24 h to generate an uptake equilibrium. The product was then centrifuged, washed with excess EtOH to purge the absorbed Cur molecules on the surface, and dried at 80 °C upon vacuum for 24 h to achieve Cur@ZIF-68 with the maximum adsorption capacity of 720.1 mg g^{-1}. Notably, to affirm this maximum uptake capacity and calculate the DLC and DLE values, Cur@ZIF-68 (3 mg) was digested in a solution containing EtOH (30 mL) and 2 M HCl (0.75 mL). The extract was then measured by UV-vis analysis to determine the total Cur content inside the ZIF-68 material. As expected, the DLC and DLE are 42.0% and 35.2%, respectively, which is in high agreement with the previously mentioned isothermal result. Continuously, 5 mg of the fabricated Cur@ZIF-68 sample is immersed and shaken in the phosphate buffer solutions at pH 7.4 and 5.0 at 37 °C, as indicated in Fig. 9a. It is noted that the release profile of ZIF-68 reveals that the Cur release rate of Cur@ZIF-68 in physiological medium is lower than that in an acidic environment, displaying the dominant pH-responsive features. This situation can be accounted for by the deprotonation of the ligands, leading to the decomposition of the coordination bonds between the Zn^{2+} ions and the linkers under acidic conditions and causing the structural order loss of Cur@ZIF-68 at pH = 5.0 after 120 h, as observed by the PXRD pattern (Fig. S5).

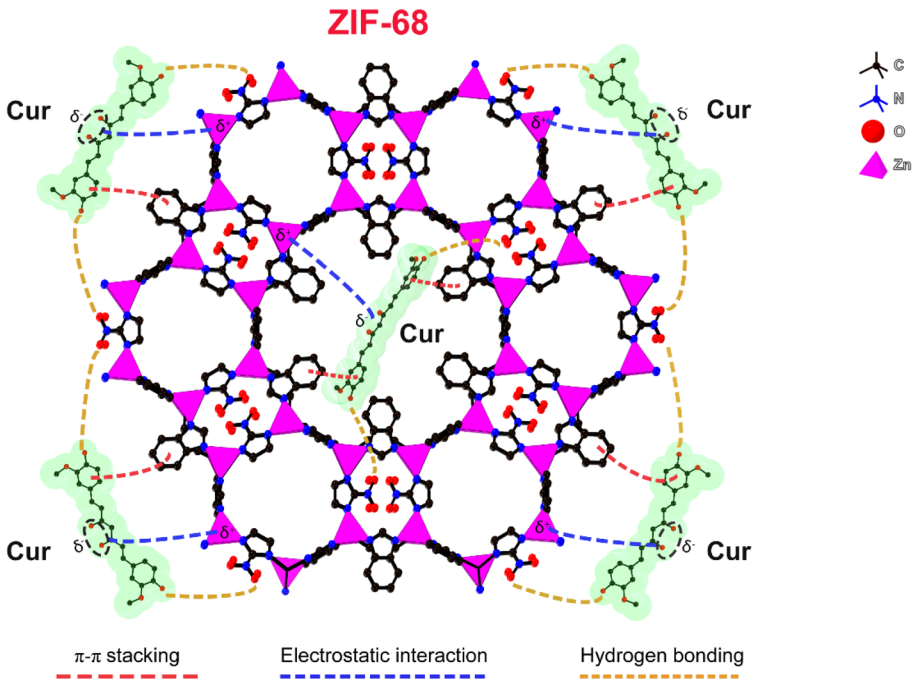

Scheme 1 The proposed uptake mechanism of Cur onto ZIF-68. Atom colors: Zn, pink polyhedra; C, black; O, red; N, blue. Almost H atoms are omitted for clarity.

Accordingly, the cumulative Cur release at pH 7.4 is 36.1% for 6 h, 43.3% for 24 h and reaches 54.1% for 132 h, which is 18.8, 23.7 and 40.9% lower than at pH 5.0 under the similar periods (Fig. 9a). The unique pH-responsive release performance of ZIF-68 in both mediums will prevent the rapid Cur release at initial stage, resulting in the efficient improvement of the cancer cell treatment possibility. Despite exhibiting a specific pH-responsive trend, the stated *in vitro* data are preliminary and do not account for physiological factors such as enzymes and serum proteins. Further *in vivo* experiments are required to assess the long-term stability and degradation behavior of the material in more complicated biological media. The achievable results demonstrated again the formation of the aforementioned strong interactions between the drug guest molecules and the ZIF backbone, as well as the relevant pore diameter of ZIF-68, supporting the controlled Cur release process to efficiently inhibit the burst effect.

To gain a deeper insight into the Cur release mechanism, the kinetic models such as zero-order, first-order, Higuchi, Korsmeyer–Peppas, and Hixson–Corwell were used. The linear fittings of the release models are described in the eqn (S10)–(S14). For further meaning of zero-order model, the drug release is only a function of the rate constant and time, driving the same amount of drugs released after the various intervals. Meanwhile, the first-order model points out that the release rate is proportional to the remaining drug content within the platform material. The Higuchi model assumes that the drug's solubility in the solution is lower than its initial concentration within the material. Also, the drug diffusion is unidirectional, the edge effect is not pronounced, and the drug particle size is smaller than the system thickness. The Korsmeyer–Peppas model is a semi-empirical model to depict the multiple release phenomena that take place simultaneously. A vital parameter of this model is n, a release exponent, which represents the drug release mechanism. As $n \leq 0.5$, the drug release corresponds to the Fickian diffusion, exhibiting a diffusion-controlled release. Whereas the intermediate values ($0.5 < n < 1$) show anomalous or non-Fickian transport, implying the drug release is driven by the structural swelling/relaxation/rearrangement and diffusion. Finally, the Hixson–Crowell model displays the surface area and particle size of the drug transport material changed throughout the drug release. This model highlights that the carrier is gradually dissolved as the discharged drug, causing a decrease in particle size over time.[54,59] Subsequently, the obtained data from the Cur release experiments of ZIF-68 incorporated with the various kinetic models are clearly shown in Fig. S6 and S7. As a result, for pH 5.0/7.4, the calculated R^2 coefficient for fitting in the Korsmeyer–Peppas model (0.993/0.995) is greater than the zero-order (0.864/0.890), first-order (0.989/0.919), Higuchi (0.954/0.980), and Hixson–Crowell model (0.989/0.910), respectively. Additionally, the n parameter achieved from the Korsmeyer–Peppas model is 0.18 and 0.13 for pH 5.0 and 7.4, respectively. These values correspond to the quasi-Fickian diffusion mechanism as a dominant driving force for the Cur release from the ZIF-68 framework at both pH environments.[60]

3.5. *In vitro* biocompatible and cytotoxicity studies

To assess the prospect performance of ZIF-68 as a drug nanocarrier platform for breast cancer cell treatment, *in vitro* biocompatibility and cytotoxicity experiments were carried out. As previously mentioned in the discussion, Cur@ZIF-68

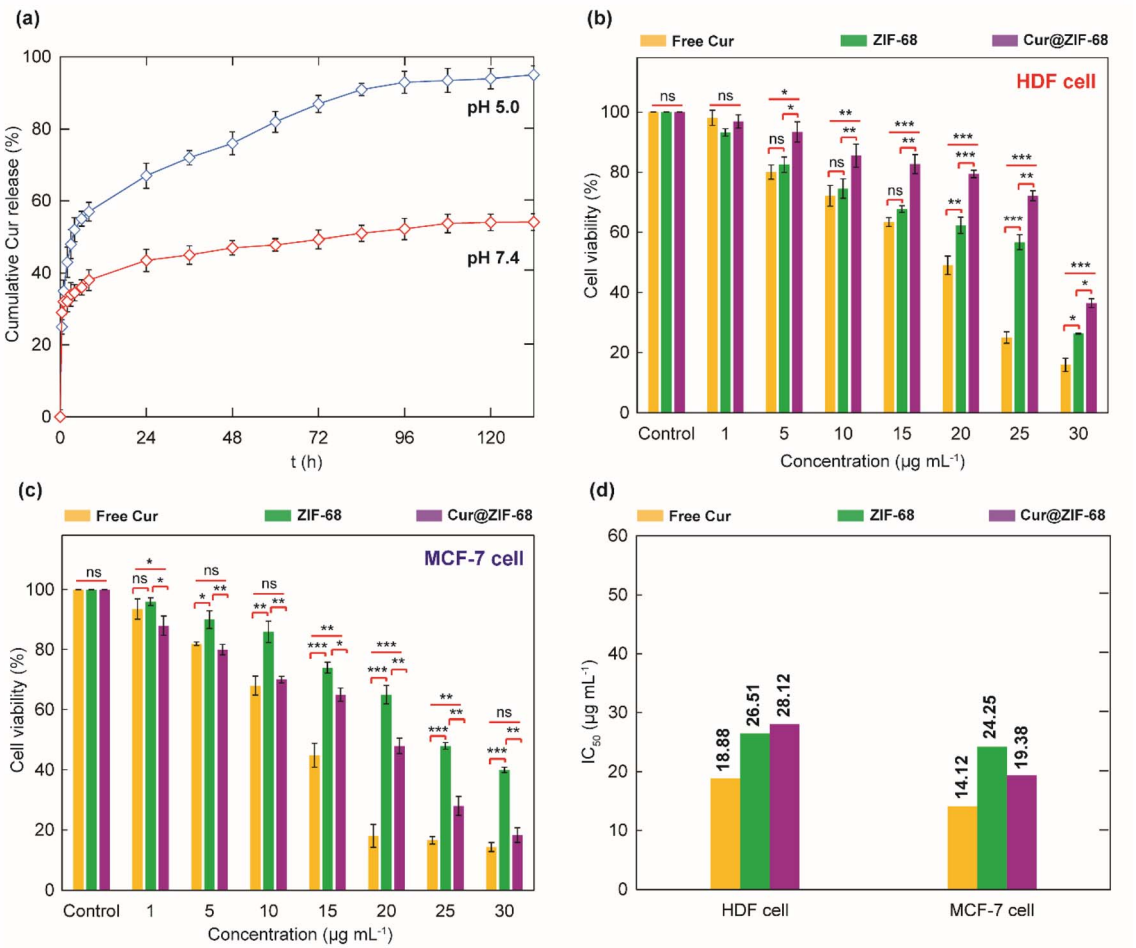

Fig. 9 Cumulative Cur release of Cur@ZIF-68 at pH 7.4 (red) and 5.0 (blue) (a); cytotoxicity of free Cur, ZIF-68, and Cur@ZIF-68 in HDF cells (b) and MCF-7 cells (c); the p-value was confirmed by unpaired two-tailed t-tests ($p < 0.05$ (*), $p < 0.01$ (**), $p < 0.001$ (***), and ns: no significant); the IC_{50} values of free Cur, ZIF-68, and Cur@ZIF-68 were calculated from the cytotoxicity toward HDF and against MCF-7 cell lines (d).

possesses the unique properties, including controlled release rate with extraordinary pH-responsive degradation property, and suitable particle size, which enable selective drug release in the tumor microenvironment, resulting in the improvement of the resistance ability toward the cancer cells and minimizing toxicity to the normal cells.

In this contribution, the cytotoxicity of the ZIF-based drug delivery system is estimated utilizing the colorimetric assays with the WST-1 reagent, which is generally employed to determine the cell viability and cytotoxicity derived from the metabolic activity of the living cells. Different from the MTT assay, which generates insoluble formazan crystals in water, demanding an additional dissolution stage, WST-1 forms water-soluble formazan crystals, leading to a shorter protocol, more sensitive, and less cytotoxic to the cells.[61] Accordingly, seven various concentrations of the free Cur, ZIF-68, and Cur@ZIF-68, ranging from 1 to 30 μg mL^{-1} in comparison with the control sample, were experimented on both HDF and MCF-7 cell lines. As given in Fig. 9b, three of the samples indicate a dose-dependent cytotoxicity by decreased cell viability and proliferation after 24 h incubation with the HDF cells. In detail, Cur@ZIF-68 maintains the cell viability with a high level up to 74.2% and 80.0% at the concentration ranges of 25 and 20 μg mL^{-1}, respectively, whereas the remaining two samples show a relatively significant decline in biocompatibility with approximately 25.1% and 56.8% cell viability for the free Cur and pure ZIF-68 at 25 μg mL^{-1}, respectively. This can be ascribed to the initial prompt burst release of the free Cur molecules and the effect of the nitro moieties inside ZIF-68 at a relatively high concentration, which can cause the rapid inhibition and damage to the normal cells. In contrast, the Cur@ZIF-68 carrier demonstrates a much lower cytotoxicity towards the HDF cells, which can be attributed to its sustained and controlled drug release performance after 24 h. Notably, it is realized that there are differences in the cytotoxicity towards the normal cell between ZIF-68 and Cur@ZIF-68 at the high dose range from 10 to 25 μg mL^{-1}. This can be explained by the following factors: (i) at the relatively high doses, ZIF-68 possesses a higher density of the nitro groups in its structure, causing a relative increase in the toxicity to the HDF cells; (ii) the Cur molecules inside the pores of the ZIF material contributed to locking/covering in the activity of the nitro groups within ZIF-68 through ultra-high

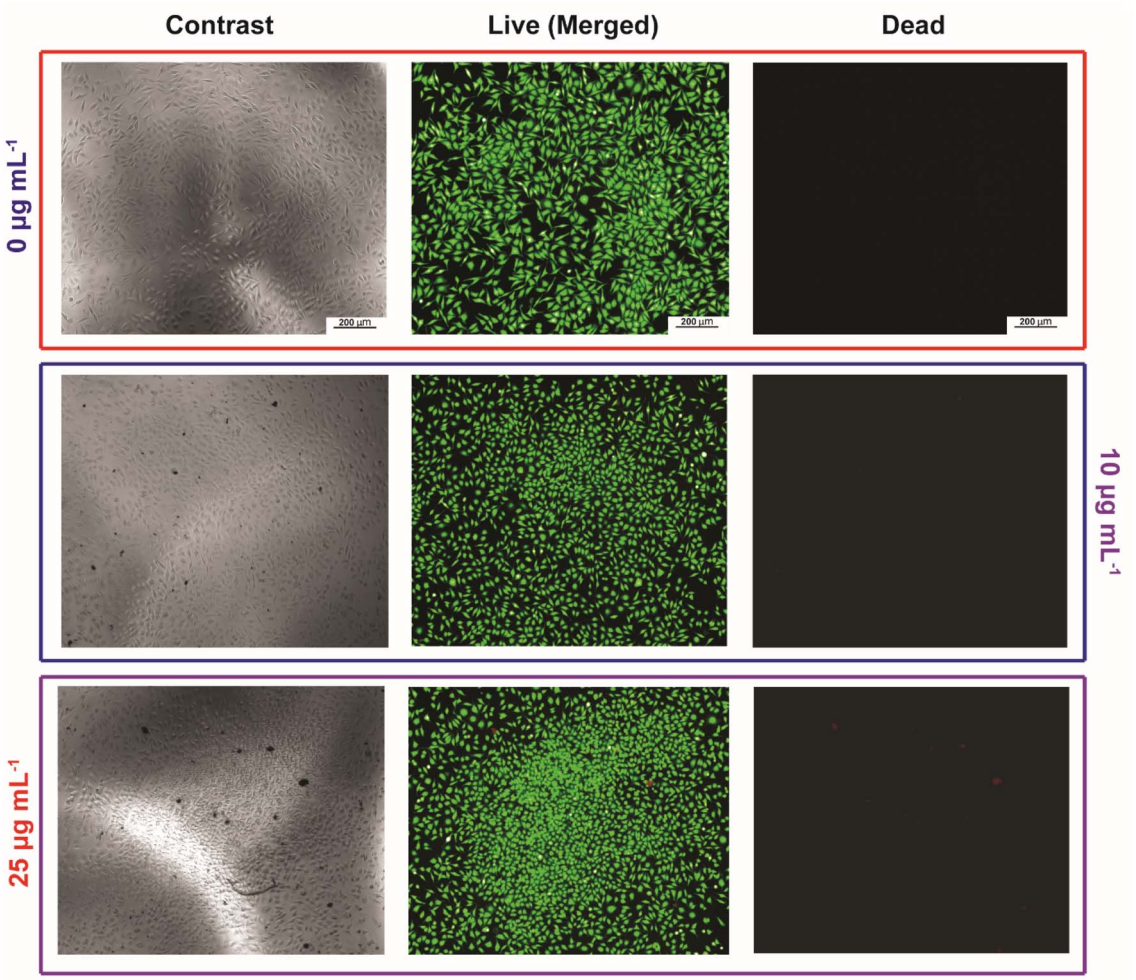

Fig. 10 Live/Dead cell staining assay images of calcein-AM and ethidium homodimer-1 stained the HDF normal cells treated with Cur@ZIF-68 at the concentration ranges of 0, 10, and 25 μg mL^{-1}. Scale bar = 200 μm.

encapsulation by forming strong interactions as mentioned. This discovery opens up novel research to enhance the biocompatible possibility through the capturing of the drug molecules onto the porous material structure containing the functional groups capable of causing cytotoxicity at high dose ranges. Interestingly, the trends in cell morphology and survival rates of the samples as compared to the control group are clearly revealed in bright-field microscopy images (Fig. S8 and S9). Additionally, the IC_{50} values of the free Cur, ZIF-68, and Cur@ZIF-68 are 18.88, 26.51, and 28.12 μg mL^{-1}, respectively (Fig. 9d), which is in good accordance with the stated data. All achievable evidence proves that the Cur@ZIF-68 material possesses a high biocompatible ability towards the normal cell line with an acceptable cell viability degree at the high doses, which is recognized in the reported works,[32,62–64] and the standard ISO 10993-5. Subsequently, for the MCF-7 cell, the IC_{50} value of ZIF-68 is 24.25 μg mL^{-1}, which is higher than Cur@ZIF-68 (19.38 μg mL^{-1}). In particular, the cell viability of the Cur@ZIF-68 sample reaches 28.1% at 25 μg mL^{-1} and 18.3% at 30 μg mL^{-1} concentration, while for the pristine ZIF-68, the cytotoxicity against the MCF-7 cell line is 48.1% and 40.4%, respectively (Fig. 9c and Table S4). This suggests that the Cur@ZIF-68 carrier indicated a greater cytotoxicity as compared to the parent ZIF-68 after 24 h. For the free Cur, the IC_{50} parameter is determined to be 14.12 μg mL^{-1} after 24 h of the therapeutic testing for the MCF-7 cell. At first glance, the IC_{50} value of the free Cur is lower than that of ZIF-68 and Cur@ZIF-68, driving a higher resistance against the breast cancer cells. Nevertheless, the actual Cur content within the Cur@ZIF-68 nanocarrier is calculated as 8.14 μg mL^{-1} with a drug loading content of 42%, which is much smaller than the free Cur IC_{50} value. It is worth noting that the encapsulation of Cur into the ZIF-68 framework indicates a significantly enhanced anticancer efficiency in comparison with the free Cur on a dose-normalized basis. Furthermore, Cur@ZIF-68 can minimize the burst effect and facilitate the sustained drug release, resulting in the enhancement of the therapeutic activity. This drug delivery system could reduce the requirement for frequent use, which generally causes systemic toxicity and undesirable side effects.

To provide a more visual and intuitive understanding of the high biocompatible property of Cur@ZIF-68 at the dose ranges of 0, 10, and 25 μg mL^{-1} toward the normal cell, a Live/Dead

assay was performed by staining with the calcein acetoxymethyl (AM) reagent to evaluate the cell morphology and viability. Herein, the staining mechanism is conducted through the reagents, such as calcein-AM and ethidium homodimer-1. Calcein-AM is capable of traveling through the intact cell membrane and is hydrolyzed by intracellular esterases in active cells to create green fluorescence, indicating living cells. Meanwhile, ethidium homodimer-1 can not pass through the intact cell membranes and only penetrates the cells owing to the damaged membranes to generate the red fluorescence, showing the dead cells. As illustrated in Fig. 10, there is no remarkable change in the cell morphology and viability observed through the dispersion of green and red fluorescence in the pictures for the Cur@ZIF-68 samples in the concentration range of 10 and 25 μg mL^{-1}, relating to the control sample (0 μg mL^{-1}), which corresponds to the surveyed cytotoxicity experiment. This finding points out that Cur@ZIF-68 could be used as a highly biocompatible drug nanocarrier for further *in vivo* assay.

4. Conclusion

In summary, a Zn-based ZIF with GME topology, termed ZIF-68, containing the nitro moieties and benzene rings incorporated with a suitable pore window size, capable of effective curcumin encapsulation, was successfully fabricated and investigated for its biocompatible performance towards normal cells and cytotoxicity against the breast cancer cell line. It is realized that the maximum uptake capacity for the Cur molecules over ZIF-68 is obtained as 720.1 mg g^{-1}, corresponding to the DLC calculation of 42%. To the best of our knowledge, this value is much greater than the previously published Cur carriers. Besides, the results from the uptake isothermal and kinetic models indicate that the Cur encapsulation is closely related to the Langmuir isotherm and the pseudo-second-order models, suggesting that the adsorption behavior follows model-based interpretations typically associated with chemical interactions. In addition, the Cur anchoring mechanism is interpreted *via* the combined analyses, indicating the formation of strong attractions such as the electrostatic and π–π interactions, and hydrogen bonding during the adsorption. Furthermore, the Cur@ZIF-68 carrier possesses the desirable controlled Cur release rate, which efficiently suppresses the drug burst phenomenon at the initial stage and the side effects caused by the free drug. In particular, the *in vitro* cytotoxicity experiments prove that Cur@ZIF-68 has a good biocompatible possibility for the HDF normal cells, and the high cytotoxicity against the MCF-7 cancer cell lines with a low IC_{50} value of 19.38 μg mL^{-1}. These findings reveal that ZIF-68 is a dominant candidate to be employed as a potential drug delivery system with high biocompatibility and effective anti-cancer therapy, leading to opening up a new horizon for scientists in the design of porous drug nanocarriers for further *in vivo* assays.

Author contributions

My Van Nguyen formulated this project. My Van Nguyen, Duy Ba Nguyen, Phuong Bich Tran, Quynh Ngoc Thi Luong, Viet Ngoc Huynh, Anh Ngoc Thi Phan, Vu Tuyet Luu, Duong Hoang Dang, Hung Ngoc Nguyen, Loc Cam Luu and Tan Le Hoang Doan synthesized the compounds and collected isotherms, powder X-ray diffraction patterns, FT-IR spectra, Raman spectra, TGA analysis. My Van Nguyen wrote the paper and all authors contributed to revising it. All authors have given approval to the final version of the manuscript.

Conflicts of interest

The authors declare no competing financial interest.

Data availability

The data used to support the findings of this study are included within the article.

Supplementary information (SI) is available. See DOI: https://doi.org/10.1039/d6ra02515c.

Acknowledgements

This research is funded by Ho Chi Minh City University of Education Foundation for Science and Technology under grant number CS.2025.19.06TĐ.

References

1 Q.-Q. Wang, Z.-P. Yang, Z.-T. Cui, X.-H. Wang and Y. Lin, A microporous Co(II)-MOF as a pH-responsive 5-FU delivery system to induce human hemangioma cells apoptosis and abrogate their growth, *J. Coord. Chem.*, 2020, **73**, 1436–1449.
2 M. Zeng, D. Guo, G. Fernández-Varo, X. Zhang, S. Fu, S. Ju, H. Yang, X. Liu, Y.-C. Wang, Y. Zeng, G. Casals and E. Casals, The integration of nanomedicine with traditional Chinese medicine: drug delivery of natural products and other opportunities, *Mol. Pharmaceutics*, 2020, **20**, 886–904.
3 C. Feng, Y. Wang, J. Xu, Y. Zheng, W. Zhou, Y. Wang and C. Luo, Precisely tailoring molecular structure of doxorubicin prodrugs to enable stable nanoassembly, rapid activation, and potent antitumor effect, *Pharmaceutics*, 2024, **16**, 1582.
4 I. O. Alisi, A. Uzairu, S. E. Abechi and S. O. Idris, Evaluation of the antioxidant properties of curcumin derivatives by genetic function algorithm, *J. Adv. Res.*, 2018, **12**, 47–54.
5 M. U. Akbar, K. M. Zia, M. S. H. Akash, A. Nazir, M. Zuber and M. Ibrahim, In-vivo antidiabetic and wound healing potential of chitosan/alginate/maltodextrin/pluronic-based mixed polymeric micelles: curcumin therapeutic potential, *Int. J. Biol. Macromol.*, 2018, **120**, 2418–2430.
6 Y. He, Y. Yue, X. Zheng, K. Zhang, S. Chen and Z. Du, Curcumin, inflammation, and chronic diseases: how are they linked?, *Molecules*, 2015, **20**, 9183–9213.
7 S. Hewlings and D. Kalman, Curcumin: a review of its' effects on human health, *Foods*, 2017, **6**, 92.
8 M. M. Yallapu, P. K. B. Nagesh, M. Jaggi and S. C. Chauhan, Therapeutic applications of curcumin nanoformulations, *AAPS J.*, 2015, **17**, 1341–1356.

9 M. Chang, M. Wu and H. Li, Antitumor Effects of Curcumin and Glycyrrhetinic Acid-modified Curcumin-Loaded Cationic Liposome by Intratumoral Administration, *J. Evidence-Based Complementary Altern. Med.*, 2020, **2020**, 1–14.

10 P. Qiu, S. Man, J. Li, J. Liu, L. Zhang, P. Yu and W. Gao, Overdose intake of curcumin initiates the unbalanced state of bodies, *J. Agric. Food Chem.*, 2016, **64**, 2765–2771.

11 J. Ma, Y. Hai, K. Ni and X. Hu, 3D printing technology: Driving pioneering innovations in anti-cancer drug delivery systems, *Int. J. Bioprint.*, 2025, **11**, 25–56.

12 A. Azevedo, M. P. Coelho, J. O. Pinho, P. I. Soares, C. P. Reis, J. P. Borges and M. M. Gaspar, An alternative hybrid lipid nanosystem combining cytotoxic and magnetic properties as a tool to potentiate antitumor effect of 5-fluorouracil, *Life Sci.*, 2024, **344**, 122558.

13 X. Ji, Z. Yang, J. Fang and S. Hu, Molecularly imprinted polymers based on attapulgite and sustained-release properties for 5-FU, *Colloid Polym. Sci.*, 2024, **302**, 1–10.

14 S. S. Kamar, D. H. Abdel-Kader and L. A. Rashed, Beneficial effect of curcumin nanoparticles-hydrogel on excisional skin wound healing in type-I diabetic rat: histological and immunohistochemical studies, *Ann. Anat.*, 2019, **222**, 94–102.

15 S. Jambhrunkar, S. Karmakar, A. Popat, M. Yu and C. Yu, Mesoporous silica nanoparticles enhance the cytotoxicity of curcumin, *RSC Adv.*, 2014, **4**, 709–712.

16 T. Feng, Y. Wei, R. J. Lee and L. Zhao, Liposomal curcumin and its application in cancer, *Int. J. Nanomed.*, 2017, **12**, 6027–6044.

17 M. A. Beach, U. Nayanathara, Y. Gao, C. Zhang, Y. Xiong, Y. Wang and G. K. Such, Polymeric nanoparticles for drug delivery, *Chem. Rev.*, 2024, **124**, 5505–5616.

18 L. Xie, L. Liu, S. Xu, T. Wang, X. Yue and G. Li, An efficient voltammetric sensing platform for trace determination of Norfloxacin based on nanoplate-like α-zirconium phosphate/carboxylated multiwalled carbon nanotube nanocomposites, *Microchem. J.*, 2024, **206**, 111451.

19 L. Dong, J. Ding, L. Zhu, Y. Liu, X. Gao and W. Zhou, Copper carbonate nanoparticles as an effective biomineralized carrier to load macromolecular drugs for multimodal therapy, *Chin. Chem. Lett.*, 2023, **34**, 108192.

20 W. Qiu, J. Fan, W. Tao, J. Liang, C. Xiao, Y. Chen, C. Tong and B. Liu, Cinobufagin loaded Prussian blue-like nanoparticles for chemo/gas therapy of multidrug resistant cancer, *J. Nanobiotechnol.*, 2025, **23**, 706.

21 M. V. Nguyen, H. K. Duong, H. N. Nguyen, L. C. Luu and T. M. Nguyen, A new MIL-101-type chromium-based metal–organic framework with densely packed sulfonic groups: an ultra-high uptake of toxic Pb^{2+} and Cu^{2+} ions from an aqueous medium, *Nanoscale Adv.*, 2025, **7**, 5104.

22 H. M. N. Pham, A. V. Phan, A. N. Phan, V. P. Nguyen, K. M. Nguyen, H. N. Nguyen, T. M. Nguyen and M. V. Nguyen, Engineering of efficient functionalization in a zirconium-hydroxyl-based metal–organic framework for an ultra-high adsorption of Pb^{2+} ions from an aqueous medium: an elucidated uptake mechanism, *Mater. Adv.*, 2024, **5**, 5118–5133.

23 R. M. Rego, G. Sriram, K. V. Ajeya, H. Y. Jung, M. D. Kurkuri and M. Kigga, Cerium based UiO-66 MOF as a multipollutant adsorbent for universal water purification, *J. Hazard. Mater.*, 2021, **416**, 125941.

24 D. T. Nguyen, H. N. Nguyen, T. M. Nguyen, H. C. Dong, N. N. Dang, Q. H. Tran, T. A. Nguyen, M. V. Tran, T. L. H. Doan, L. C. Luu and M. V. Nguyen, An excellent photodegradation efficiency of methylene blue and rhodamine B dyes in a series of porphyrinic aluminum-based MOFs metallated by copper and cobalt metals, *Colloids Surf., A*, 2024, **689**, 133663.

25 M. V. Nguyen, V. T. Luu and A. T. D. Phan, An excellent photochemical reduction property of Cr(VI) upon visible light illumination in a hydroxyl-functionalized zirconium-based metal–organic framework, *Mater. Adv.*, 2025, **6**, 4817–4832.

26 H. Liang, X. Jiao, C. Li and D. Chen, Flexible self-supported metal-organic framework mats with exceptionally high porosity for enhanced separation and catalysis, *J. Mater. Chem. A*, 2018, **6**, 334–341.

27 M. V. Nguyen, T. U. Kim, L. H. T. Nguyen, A. Mirzaei, A. T. T. Pham, T. Q. Tran, D. X. N. Mai, Q. N. Tran, Y. Kim, T. B. Phan, H. W. Kim, S. S. Kim and T. L. H. Doan, Efficient low-temperature detection of CO gas by various metalated porphyrinic-Al-based MOF (Cu and Co) materials, *Sens. Actuators, B*, 2025, **424**, 136915.

28 T. L. H. Doan, T. U. Kim, Y. Kim, M. V. Nguyen, A. Mirzaei, N. X. D. Mai, L. T. H. Nguyen, V. H. N. Tran, H. V. Nguyen, M. N. Q. Tran, T. B. Phan, H. W. Kim and S. S. Kim, Synthesis, characterization, and ethanol vapor sensing characteristics of vanadium-based-MOFs with and without Cu doping, *Chem. Eng. J.*, 2026, **529**, 172679.

29 L. E. Kreno, K. Leong, O. K. Farha, M. Allendorf, R. P. V. Duyne and J. T. Hupp, Metal-organic framework materials as chemical sensors, *Chem. Rev.*, 2012, **112**, 1105–1125.

30 S. Li, S. Ma, J. Sun, Y. Zhang, Z. A. Wang, L. Sheng, B. Jiang, Q. Liu and L. Jin, Zirconium metal-organic cage integrated with fluorescein sodium: a dye-functionalized dual-emission platform for ratiometric sensing of sunset yellow, *Dyes Pigm.*, 2026, **249**, 113628.

31 A. T. Duong, H. V. Nguyen, M. V. Tran, Q. N. Ngo, L. C. Luu, T. H. L. Doan, H. N. Nguyen and M. V. Nguyen, Influence of ZIF-9 and ZIF-12 structure on the formation of a series of new co/n-doped porous carbon composites as anode electrodes for high-performance lithium-ion batteries, *RSC Adv.*, 2023, **13**, 17370–17383.

32 S. Mirzanejad, M. Bagherzadeh, A. Bayrami, H. Daneshgar, A. Bahrami and M. Mahdavi, Improving the drug delivery performance of ZIF-8 with amine functionalization as a 5-fluorouracil nanocarrier, *Sci. Rep.*, 2025, **15**, 18793.

33 D. S. Khafaga, M. T. El-Morsy, H. Faried, A. H. Diab, S. Shehab, A. M. Saleh and G. A. Ali, Metal–organic frameworks in drug delivery: engineering versatile platforms for therapeutic applications, *RSC Adv.*, 2024, **14**, 30201–30229.

34 H. Furukawa, K. E. Cordova, M. O'Keeffe and O. M. Yaghi, The chemistry and applications of metal-organic frameworks, *Science*, 2013, **341**, 1230444.
35 J. Chen, C. Wang, Z. Y. Zhu, F. Wang, J. Shang, Z. Liu and L. Wang, Titanium-based metal-organic frameworks as pH-responsive drug delivery carriers of 5-fluorouracil, *J. Solid State Chem.*, 2024, **332**, 124563.
36 Y. Nie, D. Li, Y. Peng, S. Wang, S. Hu, M. Liu, J. Ding and W. Zhou, Metal organic framework coated MnO_2 nanosheets delivering doxorubicin and self-activated DNAzyme for chemo-gene combinatorial treatment of cancer, *Int. J. Pharm.*, 2020, **585**, 119513.
37 Q. Wang, Y. Sun, S. Li, P. Zhang and Q. Yao, Synthesis and modification of ZIF-8 and its application in drug delivery and tumor therapy, *RSC Adv.*, 2020, **10**, 37600–37620.
38 N. Motakef-Kazemi, S. A. Shojaosadati and A. Morsali, Evaluation of the effect of nanoporous nanorods $Zn_2(BDC)_2(DABCO)$ dimension on ibuprofen loading and release, *J. Iran. Chem. Soc.*, 2016, **13**, 1205–1212.
39 D. Y. Ma, J. M. Xie, Z. W. Zhu, H. L. Huang, Y. T. Chen, R. X. Su and H. M. Zhu, Drug delivery and selective CO_2 adsorption of a bio-based porous zinc-organic framework from 2,5-furandicarboxylate ligand, *Inorg. Chem. Commun.*, 2017, **86**, 128–132.
40 S. Yu, S. Wang, Z. Xie, S. Yu, L. Li, H. Xiao and Y. Song, Hyaluronic acid coating on the surface of curcumin-loaded ZIF-8 nanoparticles for improved breast cancer therapy: an in vitro and in vivo study, *Colloids Surf., B*, 2021, **203**, 111759.
41 K. Chotchindakun, N. Setthaya, C. Chindawong, W. G. Song, C. Manaspon and P. Mekrattanachai, Liposome layer engineering of CCM@ZIF-8: a strategy for enhanced biocompatibility and controlled release in cancer therapy, *J. Drug Delivery Sci. Technol.*, 2026, **115**, 107616.
42 A. Kasik, X. Dong and Y. S. Lin, Synthesis and stability of zeolitic imidazolate framework-68 membranes, *Microporous Mesoporous Mater.*, 2015, **204**, 99–105.
43 Y. Liu, A. Kasik, N. Linneen, J. Liu and Y. S. Lin, Adsorption and diffusion of carbon dioxide on ZIF-68, *Chem. Eng. Sci.*, 2014, **118**, 32–40.
44 T. A. Nguyen, Q. D. Tang, D. C. T. Doan and M. C. Dang, Micro and nano liposome vesicles containing curcumin for a drug delivery system, *Adv. Nat. Sci.: Nanosci. Nanotechnol.*, 2016, **7**, 035003.
45 S. Tanaka, K. Fujita, Y. Miyake, M. Miyamoto, Y. Hasegawa, T. Makino, S. Van der Perre, J. C. S. Remi, T. V. Assche, G. V. Baron and J. F. Denayer, Adsorption and diffusion phenomena in crystal size engineered ZIF-8 MOF, *J. Phys. Chem. C*, 2015, **119**, 28430–28439.
46 V. V. Butova, V. A. Polyakov, E. A. Bulanova, M. A. Soldatov, I. S. Yahia, H. Y. Zahran, A. F. A. El-Rehim, H. Algarni, A. M. Aboraia and A. V. Soldatov, MW synthesis of ZIF-65 with a hierarchical porous structure, *Microporous Mesoporous Mater.*, 2020, **293**, 109685.
47 S. Van der Perre, T. Van Assche, B. Bozbiyik, J. Lannoeye, D. E. De Vos, G. V. Baron and J. F. Denayer, Adsorptive characterization of the ZIF-68 metal-organic framework: a complex structure with amphiphilic properties, *Langmuir*, 2014, **30**, 8416–8424.
48 H. Wang, M. Gu, X. Huang, A. Gao, X. Liu, P. Sun and X. Zhang, Ligand-based modulation of the electronic structure at metal nodes in MOFs to promote the oxygen evolution reaction, *J. Mater. Chem. A*, 2023, **11**, 7239–7245.
49 R. L. Papurello, L. A. Lozano, E. V. Ramos-Fernández, J. L. Fernández and J. M. Zamaro, Post-synthetic modification of ZIF-8 crystals and films through UV light photoirradiation: impact on the physicochemical behavior of the MOF, *ChemPhysChem*, 2019, **20**, 3201–3209.
50 Y. S. A. Aziz, A. Liu, S. Yu and B. S. Hsiao, Nitro-oxidation process for sustainable production of carboxylated lignin-containing cellulose nanofibers from sugarcane bagasse, *Carbohydr. Polym.*, 2025, **368**, 124109.
51 I. Afyouni, P. Ghanbarikondori, N. S. Pour, P. M. Hashemian, F. Jalali, A. Sedighi and M. Allahyartorkaman, Studying the characteristics of curcumin-loaded liposomal nanoparticles, *Asian Pac. J. Cancer Biol.*, 2024, **9**, 183–189.
52 F. Silvestre, C. Santos, V. Silva, A. Ombredane, W. Pinheiro, L. Andrade, M. Garcia, T. Pacheco, G. Joanitti, G. Luz and M. Carneiro, Pharmacokinetics of curcumin delivered by nanoparticles and the relationship with antitumor efficacy: a systematic review, *Pharmaceuticals*, 2023, **16**, 943.
53 L. G. Freidus, P. Kumar, T. Marimuthu, P. Pradeep and Y. E. Choonara, Theranostic Mesoporous Silica Nanoparticles Loaded with a Curcumin-Naphthoquinone Conjugate for Potential Cancer Intervention, *Front. Mol. Biosci.*, 2021, **8**, 670792.
54 R. Karimi Alavijeh and K. Akhbari, Biocompatible MIL-101(Fe) as a smart carrier with high loading potential and sustained release of curcumin, *Inorg. Chem.*, 2020, **59**, 3570–3578.
55 M. Zheng, S. Liu, X. Guan and Z. Xie, One-step synthesis of nanoscale zeolitic imidazolate frameworks with high curcumin loading for treatment of cervical cancer, *ACS Appl. Mater. Interfaces*, 2015, **7**, 22181–22187.
56 S. Jung, S. Chang, N. E. Kim, S. O. Choi, Y. J. Song, Y. Yuan and J. Kim, Curcumin/zeolitic imidazolate framework-8 nanoparticle-integrated microneedles for pH-responsive treatment of skin disorders, *ACS Appl. Nano Mater.*, 2022, **5**, 13671–13679.
57 I. N. Reddy, K. Mallikarjuna, A. A. Ghfar, P. Rosaiah, B. Akkinepally, M. Dhanasekar, J. Shim and C. Bai, Photoelectrochemical charge kinetics and transfer mechanisms of organic curcumin (turmeric) photoelectrodes, *J. Appl. Electrochem.*, 2024, **54**, 2637–2647.
58 M. Rahman, M. Kabir, T. Islam, Y. Wang, Q. Meng, H. Liu, S. Chen and S. Wu, curcumin-loaded ZIF-8 nanomaterials: exploring drug loading efficiency and biomedical performance, *ACS Omega*, 2025, **10**, 3067–3079.
59 E. E. Çalışkan, Y. Ç. Aydın, E. N. Ozbek, I. Alcın, E. Kilinc, G. Y. Anacak and E. O. C. Uyanikgil, In vitro drug release kinetics and antioxidant activity of metformin-loaded niosomes, *ACS Omega*, 2025, **10**, 58225–58237.
60 P. N. Dave, P. M. Macwan and B. Kamaliya, Biodegradable Gg-*cl*-poly(NIPAm-*co*-AA)/-*o*-MWCNT based hydrogel for

combined drug delivery system of metformin and sodium diclofenac: in vitro studies, *RSC Adv.*, 2023, **13**, 22875–22885.
61 J. Suni, S. Valkama and E. Peltola, Save your tears for the toxicity assays carbon nanotubes still fooling scientists, *ACS Omega*, 2025, **10**, 5554–5562.
62 M. M. Querido, F. Rosário, M. J. Bessa, F. Mendes, J. C. Teixeira, J. P. Teixeira and C. C. Pereira, In vitro cyto- and genotoxicity assessment of antibacterial paints with triclosan and isoborneol, *Toxics*, 2022, **10**, 58.
63 K. X. Wang, M. R. Cai, D. G. Yin, X. L. Hu, H. Y. Peng, R. Y. Zhu, M. T. Liu, Y. C. Xu, C. H. Qu, J. Ni and X. B. Yin, IRMOF-8-encapsulated curcumin as a biocompatible, sustained-release nano-preparation, *Appl. Organomet. Chem.*, 2022, **36**, e6680.
64 P. Lagonegro, F. Rossi, C. Galli, A. Smerieri, R. Alinovi, S. Pinelli, T. Rimoldi, G. Attolini, G. Macaluso, C. Macaluso, S. E. Saddow and G. A. Salviati, Cytotoxicity study of silicon oxycarbide nanowires as cell scaffold for biomedical applications, *Mater. Sci. Eng., C*, 2017, **73**, 465–471.